Mode-I Fracture in Bonded Wood: Studies of Adhesive Thermal Stability, and of the Effects of Wood Surface Deactivation

by

Tian Gao

A Thesis submitted to the Faculty of

Virginia Polytechnic Institute and State University

In partial fulfillment of the requirements for the degree of

MASER OF SCIENCE

in

Wood Science and Forest Products

Charles E. Frazier, Chairman

David A. Dillard

Scott Renneckar

February 01, 2010

Blacksburg, Virginia

Keywords: Fracture Testing, Dual Cantilever Beam,

Wood Adhesion, Thermal Stability

Mode-I Fracture in Bonded Wood: Studies of Adhesive Thermal Stability, and of the Effects of Wood Surface Deactivation

Tian Gao

ABSTRACT

This work included two separate studies; the common theme in each was the use of mode-I fracture testing to evaluate wood adhesion.

In the first study, mode-I fracture testing was used to compare the thermal stability of polyurethane (PUR) and resorcinol-formaldehyde (RF) wood adhesives. Bonded specimens for both adhesives were subjected to prolonged thermal exposure, and fracture testing was subsequently conducted after re-equilibration to standard test conditions. It was found that both PUR and RF suffered a significant fracture energy loss after heat treatment, and that RF was more thermally stable than PUR, as expected. However, both adhesives suffered significant thermal degradation, and fracture testing did not distinguish the RF system as being clearly superior to PUR. Dynamic mechanical analysis (DMA) was also used to analyze and compare the thermal softening of PUR and RF in terms of the decline in storage modulus. DMA results indicated that PUR specimens suffered greater stiffness loss due to simple thermal softening. Because fracture testing indicated that both adhesives suffered significant degradation, the DMA results suggested that the generally superior fire resistance of RF adhesives is born from greater high temperature stiffness; whereas the more compliant PUR suffers greater immediate softening during thermal

exposure. In other words, both systems suffer from thermal degradation, but the more highly cross-linked RF system suffers less thermal softening and therefore maintains a greater load carrying capacity during fire exposure.

In the second study, mode-I fracture testing was used to test the effects of wood surface thermal deactivation (surface energy reduction) on the adhesion between southern pine wood (*Pinus spp*.) and polyethylene (PE). Pine specimens were progressively surface deactivated by 185°C heat treatments for periods of 5, 15, and 60 minutes. Control and deactivated pine laminae were subsequently hotpressed/bonded using PE film as the adhesive. Mode-I fracture testing was conducted under the assumption of linear elasticity, however load/displacement test curves suffered from a severe degree of nonlinearity believed to be caused by PE bridging behind the advancing crack tip. Instead of applying a nonlinear data analysis, a standard linear elastic analysis was conducted and deemed acceptable for comparative purposes within this study. Under dry conditions (unweathered specimens), 5 and 15 minute thermal treatments resulted in progressively worse adhesion (lower fracture energies) when compared to control surfaces; but the 60 minute heat treatment improved adhesion relative to 5 and 15 minute treatments, and showed a trend of improving adhesion as surface deactivation became more extreme. Simulated-weather resistance was also studied and it was determined that the highest degree of surface deactivation slightly improved weather durability in comparison to control surfaces. Overall, the findings here were similar to those in a previously published work- thermal deactivation of wood surfaces shows promise as a method to improve adhesion between wood and nonpolar polyolefins.

ACKNOWLEDGEMENTS

First, please allow me to express my topmost sincere thanks and appreciation to my advisor, Dr. Chip Frazier. Thanks for his precise guide, which made my research very effective and smooth. Thanks for his encouragement, which help me grow and instill confidence in me. Thanks for his helping in my writing skills. But, most of all, thanks for training me to be honest and objective in researching.

Also, I would like to thank all my committee members: Dr. David Dillard and Dr. Scott Renneckar for their advice and help. Additionally, I would like to thank Rick Caudill, David Jones, Debbie Garnand, Angela Riegel and all members in Wood Adhesion Group, for their help.

Last but not least, I would like to appreciate my family, who are always my best team mate supporting, admitting and encouraging me.

TABLE OF CONTENTS

LIST OF FIGURES

LIST OF TABLES

CHAPTER ONE: INTRODUCTION

Recently more attention has been paid to the thermal stability of wood adhesives because of the fire considerations of wood composite materials used in residential buildings. Wood adhesives derived from phenol/resorcinol-formaldehyde technologies are well known for their excellent thermal stability, and have dominated the wood exterior-grade wood adhesive market. Within last the 10 years, isocyanate-based adhesives and particularly polyurethane wood adhesives successfully entered the exterior-grade wood adhesive market, meaning that they met structural certification criteria which includes passing ASTM D2559-04 (2004), commonly known as the "delamination test." This test does not include the evaluation of fire performance and thermal stability. Unfortunately fire-related wood adhesive failures were reported, and the concern regarding the thermal stability of wood adhesives rose across the industry. Particularly it was well known that polyurethane wood adhesives are less thermally stable than phenolic and resorcinolic systems. Thus, a series of heat resistance standards were developed, such as ASTM D7374-08 (2008) and D7247-07ae1 (2008). Borne from these recent concerns, the focus of the first portion of this research is to investigate the thermal stability of polyurethane and resorcinol/formaldehyde adhesives using the mode-I fracture test method.

The second part of this study addresses composite materials made from wood particles and common thermoplastic polyolefin polymers. Such wood/thermoplastic materials have obtained a significant portion of the residential construction market, such as home decking and railing applications. However wood is very hydrophilic while thermoplastic

polyolefins are very hydrophobic. The dramatic difference of polarity between wood and polyolefins compromises adhesion. Since wood/thermoplastic composites are necessarily low cost and narrow profit margin materials, there is very little opportunity to apply interfacial coupling agents to improve adhesion. Follrich et al. (2006) found that polyethylene (PE) adhesion to spruce wood (*Picea abies Karst*.) can be significantly improved by reducing wood surface energy through heat treatment (thermal surface deactivation). The second portion of this research is to follow up on Follrich et al. (2006) and determine if the thermal surface deactivation of southern pine wood (*Pinus spp*.) also enhances adhesion with PE. Furthermore and not addressed by Follrich et al. (2006) is the influence of wood surface deactivation on the weather durability of wood/PE adhesion.

Mode-I fracture testing was developed by Griffith originally for brittle materials (such as glass). Ebewele et al. (1979) first applied fracture testing to study wood adhesion. In the following 25 years, efforts have focused on methods to improve and simplify the test procedure. Currently, the flat double cantilever beam (DCB) specimen is commonly used as fracture testing specimen. A significant advantage of wood adhesion fracture testing is that crack propagation is confined the bondline and very little wood failure is involved. Mode I fracture testing will be used as the major testing method in the two works introduced above. In addition, dynamic mechanical analysis (DMA), melt rheology and static contact angle measurement will also be used in this study.

CHAPTER TWO: LITERATURE REVIEW

2.1 THERMAL DEGRADATION OF WOOD

Wood in standing tree always has very high moisture content (usually higher than 75%), and must be dried before using. In addition, wood is a combustible material and can be destroyed by unwanted fires. Therefore, as structural material, thermal degradation of mechanical properties of wood is important and was studied by many researchers. Usually, the effects of heating on the strength and stiffness of wood, reflected by the modulus of rupture (MOR) and modulus of elasticity (MOE) respectively, were focus in their studies. Generally speaking, as for temperature below 100°C, the strength and stiffness of wood decrease when heated and increase when cooled. This temperature effect is immediate and, for the most part, recoverable (LeVan and Winandy, 1990; Winandy, 1996) as for long duration heating at high temperature (>100°C), the strength is permanently reduced because of degradation of wood substance with a corresponding loss in woody material and weight. The magnitude of the permanent strength reduction depends upon moisture content, heating medium, temperature, exposure period, species and specimen size (LeVan and Winandy, 1990; Winandy, 1994). The following review is focused on the permanent thermal degradation of wood due to high temperature (>100°C) heating.

Wood is composed of cell wall components and extraneous substances, commonly called extractives. The cell wall components are the structural members of the wood cell, and largely govern the physical properties of wood. The cell wall components contain 41% (45%) cellulose in softwood

(hardwood), 30% hemicellulose and 28% (22%) lignin in softwood (hardwood). White and Dietenberger (2001) reported that between 100°C and 200°C, wood becomes dehydrated, and can be charred with prolonged exposures; hemicellulose and lignin components are pyrolyzed in the ranges of 200-300°C and 225-450°C respectively; significant depolymerization of cellulose occurs in the range of 300-350°C. All wood components end their volatile emission at around 450°C. At higher 450°C, the remaining wood residue is char. LeVan and Winandy (1990) also summarized the work on wood chemistry of thermal degradation. He reported that chemical bonds in wood begin to break down at about 175°C, and temperature ranges of the thermal degradation of hemicellulose, lignin and cellulose are 200-260°C, 200-400°C and 260-350°C respectively.

It was reviewed by Salamon (1969) that increases in temperature sometimes result in decrease in mechanical properties. However, all mechanical properties are not affected in the same way, and the magnitude of reduction is related to wood species. For example, high temperature drying has only a minimal effect on MOR (+5 to -10%) and MOE (+2 to -3%) in Southern Pines (Koch, 1971, 1976; Yao and Taylor, 1979), but it has a more severe effect on MOR (-9 to -21%) and MOE (+3 to -4%) in other softwoods, notably Douglas Fir, Hem-Fir and Spruce-Pine-Fir. The limited data available on the effect of high-temperature drying on hardwoods indicate similar minimal reductions in MOR (+1 to -10) and MOE (+4 to -4) (Gerhards, 1983; Ladell, 1956; MacKay, 1976). It is noticed that although the effect of drying on MOR and MOE is very minimal, the reduction of MOR is always higher than MOE. However, it has to be known that most studies were conducted under 116°C, a common temperature for kiln-drying, and few studies have investigated the effect of temperature

above 116°C.

Limited data on the effects of heating at four temperatures above 100°C on MOR and MOE were summarized in Figure 1 and Figure 2 (Wood Hand Book-Wood as an engineering material (1999), Chapter 4). Although the rates of MOR and MOE loss increase as a function of temperature, magnitudes of reduction of MOR and MOE are different. The reduction of MOR is significant, especially at 155 and 175°C. It can be explained by that the reduction of MOR is because of the degradation of wood substance, and the degradation increase at high temperature and for long exposure time. However, the reduction of MOE is not significant, and the initial drying can even cause some increase in MOE. In conclusion, the effect of heating on MOR is more significant than MOE, especially at high temperatures where wood substance is degraded; the reduction of MOE at high temperature is very minimal and non-significant.

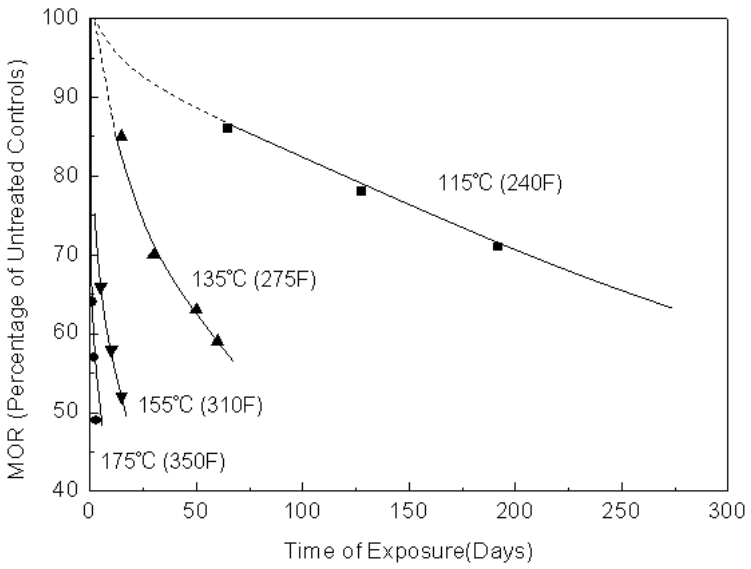

Figure 1. Permanent effect of oven heating at four temperatures on MOR, based on four clear pieces of four softwood and two hardwood species. (Adapted from Wood Hand Book-Wood as an engineering material (1999) Figure 4-17)

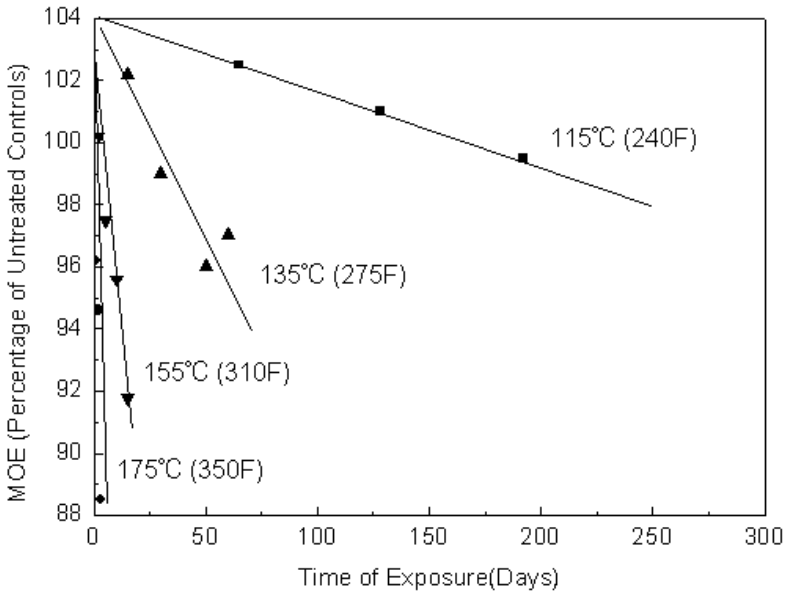

Figure 2. Permanent effect of oven heating at four temperatures on MOE, based on four clear pieces of four softwood and two hardwood species. (Adapted from Wood Hand Book-Wood as an engineering material (1999) Figure 4-17)

Another physical property of wood, that can be affected by high temperature, is equilibrium moisture content (EMC) of wood. Wood is hygroscopic material because of hydroxyl groups in cell wall components. At EMC, the wood is neither gaining nor losing moisture; the flux of water molecule into cell wall is exactly balanced by the outward into the atmosphere. Akyildiz and Ates (2008) tested EMCs of four species of wood after heating at 130, 180 and 230°C for two different times (2 and 8 hours). They found that the EMC significantly decreases with increasing heating temperature and time. This result well fits the conclusion that heat-treated wood becomes less hygroscopic because of thermal degradation of hemicellulose and lignin (Tjeerdsma et al., 1998).

2.2 THERMAL DEACTIVATION OF WOOD SURFACES

Excessive heat treatment not only affects the mechanical properties of wood, but also changes another important character, surface energy. Wood is hydrophilic because of the numerous hydroxyl groups in the wood polymers. Excessive heating can deactivate the wood surface (reduce the surface energy); this impairs adhesive wetting and negatively impacts bondline performance (Sernek et al., 2004).

Wod thermal deactivation is dependent upon on species, moisture content, drying temperature and time (Sernek et al., 2004). For each wood species, there is a critical temperature below which the thermal deactivation is not significant (Christiansen, 1990). For example, southern pine was thermally deactivated at 160°C, while yellow popular was thermally deactivated at 180°C (Sernek et al., 2004); beech's wettability suddenly decreased at 130°C (Hakkou et al., 2005); the contact angle of fir increased as heating temperature increased from 60 to 200°C (Podgorski et al., 2000).

As for mechanisms that could cause a hydrophobic change in synthetic polymer surface, Owen et al. cited six possibilities: 1 external contamination; 2 changes in surface roughness; 3 loss of volatile oxygen-rich species from the surface to the atmosphere; 4 reorientation of surface hydrophobic polymer chains from the bulk to the surface; 5 migration of hydrophobic polymer chains from the bulk to the surface; 6 migration and deposition of low energy, low molecular weight molecules on surface. The first four are not likely to significantly affect wood (Gunnells et al., 1993). The conclusion was well accepted by researchers that the thermal deactivation of wood is because of the migration of hydrophobic

extractives. The extractives are migrated to the wood surface in water and form a thin boundary layer. But the deactivation is not one phenomenon, but several (Christiansen, 1990). For example, Sernek et al. reported that the thermal deactivation is also related to the volatile organic compounds (VOCs). During heating, VOCs was evaporated, and deposited on wood surface by condensation, because in the oven the temperature of wood surface is lower than the atmosphere. It was also found (Sernek et al., 2004) that on the wood surface, the ratio of O/C decreased and the ratio of C1/C2 (C1=carbon atoms bonded to other carbon or to hydrogen atoms; C2=carbons bonded to oxygen atoms) increased with drying temperature.

In the bonding, the water needs to be removed from the adhesive to accelerate curing. Some of the water usually diffuses into the wood bulk during the assembly time, but the deactivated surface will not let the moisture or resin easily penetrate the surface layers, and the excess water retained in the bondline slowed the cure. However, if using thermoplastic adhesive, such as polyethylene, the deactivation of wood surface can significantly improve the adhesion by reducing the difference of polarity between wood and polyethylene (Follrich et al., 2006). Also, the thermal treatment can also decrease the wood hygroscopy to improve the residual mechanical properties after outdoor weathering and dimensional stability to moisture change (Del Menezzi, et al., 2008).

2.3 FRACTURE TESTING

Prior to the development of fracture mechanics in 1950s and 1960s, engineering design was based primarily on the yield strength obtained in tension, compression and bending tests. However, people always had to

face a problem that the failure can occur at stresses below the material's yield strength, where failure would not be expected. Fracture mechanics explained that this unexpected failure was due to cracks or crack-like flaws, that are difficult to prevent. Figure 3 shows three basic modes of fracture: opening mode (mode-I), sliding mode (mode-II) and tearing mode (mode-III). Most cracking problems were caused by mode-I fracture which our discussion will be focused on.

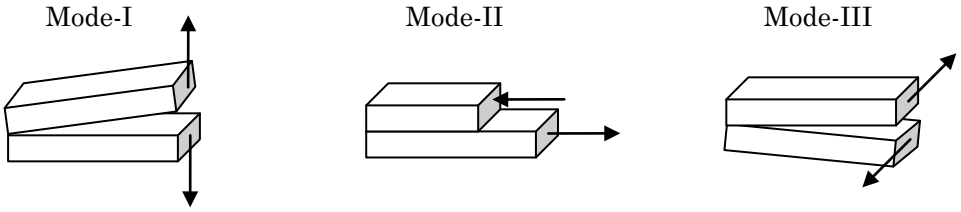

Figure 3. Three modes of fracture

Figure 4 shows the mechanism of failure below tension yield strength. Stresses are concentrated in the crack tip A, and a quantity called stress intensity factor, K, is defined as $K = 1.12S\sqrt{\pi a}$, where a is crack length infinitely smaller than the sample length, b, and S is the tension stress. K is a measure of the severity of stress concentration in crack tip as affected by crack size and stress.

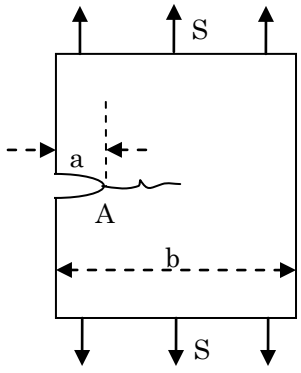

Figure 4. Crack growth in single edge under mode-I fracture

A given material can resist a crack growth as long as K is below a critical value K_c, called the fracture toughness. K_c is a material property, affected by temperature, loading rate and thickness of the member. Therefore critical tension stress S_c can be derived from K_c by Equation 1. Because this S_c was usually below the tension yield strength, much failure occurred at low stress.

$$S_c = \frac{K_c}{1.12\sqrt{\pi a}} \tag{1}$$

Figure 5 shows another measure of fracture performance with energy as the critical variable. Strain Energy Release Rate (SERR), or Fracture Energy, G, was defined as the energy per unit area required to extend a new crack.

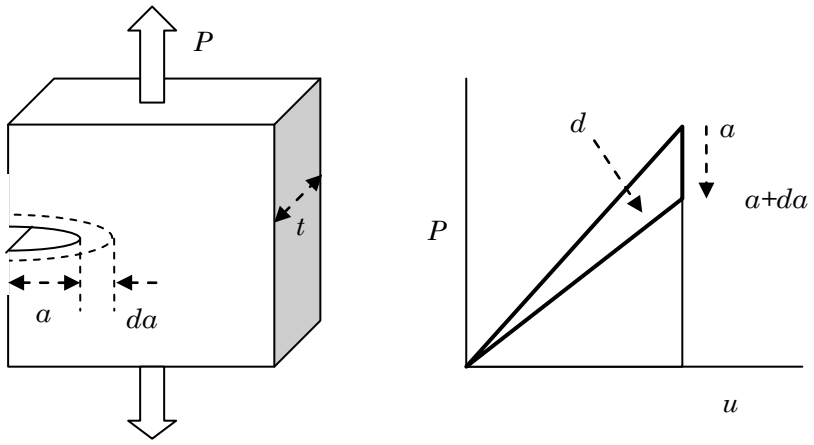

Figure 5. Strain Energy Release Rate (SERR) or Fracture Energy in Griffith's concept

Energy methods were employed in the earliest work on fracture mechanics reported by Grifiith in 1920 (Dowling, 2007). the behavior of brittle materials (such as glass) was assumed as linear-elastic, where the

relationship between load P and displacement u is linear. All energy change (dU in Figure 5), area of closed loading cycle was used in the new crack propagation. Therefore, the G was calculated as follows:

$$G = \frac{d\mathrm{U}}{\mathrm{t}da} \tag{2}$$

where t is the thickness of the member; da is the new crack length. However, in more ductile materials, some energy loss is dispersed in deforming the material in the plastic zone at the crack tip. In the 1950s, It was found that Griffith's concept was also applicable to metals if the plastic zone in the crack tip was small when G was applied.

The need for fracture testing in wood adhesive evaluation is necessary because of both internal cracks and crack-like flaws in the bondline, and the mechanical properties of wood. In traditional shear lap testing as shown in Figure 6 (a), bonding quality was difficult to test because of high percentages of wood failure, which only shows that the adhesive is stronger than wood under shear stress. In contrast, fracture testing is an especially bondline-sensitive testing method, which concentrates the failure exclusively to bondline as shown in Figure 6 (b).

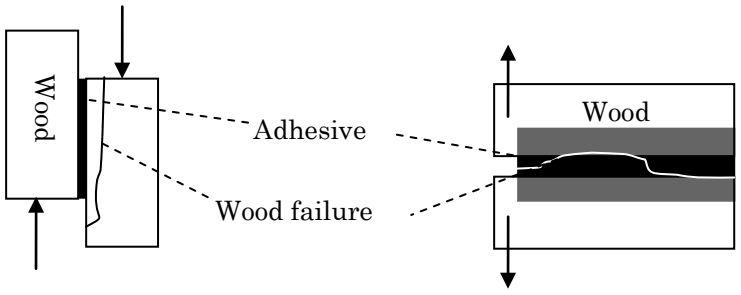

(a) Shear (b) Fracture

Figure 6. Shear testing (a) and fracture testing (b)

Ebewele et al. (1979) used the contoured Dual Cantilever Beam (DCB) method to test the effects of bondline thickness, wood anisotropy, and curing time on the fracture energy of phenolic-wood bonding. The critical strain energy release rate (fracture energy), G_{Ic}, under mode-I fracture is defined by the following relationship:

$$\mathrm{G_{Ic}} = \frac{\mathrm{P_c^2}}{2B}\left(\frac{\mathrm{dC}}{\mathrm{da}}\right) \tag{3}$$

$$\frac{\mathrm{dC}}{\mathrm{da}} = \frac{8}{\mathrm{EB}}\left[\frac{3\mathrm{a}^2}{\mathrm{h}^3} + \frac{1}{\mathrm{h}}\right] \tag{4}$$

$$m = \frac{3\mathrm{a}^2}{\mathrm{h}^3} + \frac{1}{\mathrm{h}} \tag{5}$$

$$\mathrm{G_{Ic}} = \frac{4\mathrm{P_c^2}}{\mathrm{EB}^2}\mathrm{m} \tag{6}$$

where P_c is critical load when crack extension is initiated, a is crack length, B is the width of beam, C is compliance of specimen, h is uniform height and E is bending modulus of wood.

In the experiment, the beams were contoured before bonding so that compliance changed linearly with crack length, where m in Equation 5 is constant. However, this required extensive specimen preparation. Also, due to the curvature of the beam, it was difficult to apply a constant pressure during bonding, which resulted in the non-uniform bondline thickness.

The non-uniform bondline can significantly influence the critical fracture energy. An optimum bondline thickness for hard maple/phenol-resorcinol bonding was found at roughly 85 um. It is important to note that optimum

bondline thickness is a function of the wood species and adhesive system. Sasaki et al. (1973) found the optimum bondline thickness for Karui/epoxy to be 500um.

Ebewele (1980) investigated the effects of bonding surface preparation on the fracture energy. The hand-sanded specimens had different crack path as shown in Figure 7, and higher fracture energy than machine-sanded samples; the surfaces sanded perpendicular to the crack path had higher fracture energy than those sanded parallel to the crack path; rougher surfaces sanded with harsher sandpaper had higher fracture energy. It was also determined that aging of the bonding surface can significantly decrease the fracture energy. Thus fracture energy could be increased by exposing fresh wood by re-machining surface before bonding.

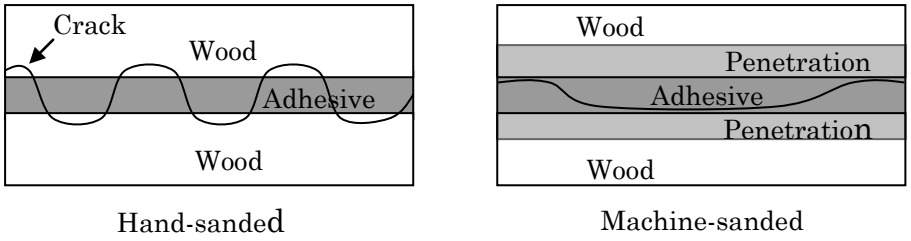

Figure 7. Difference in adhesive penetration and the crack path in hand-sanded and machine-sanded specimens

In order to obtain bonded wood products from tree, green wood must be subjected to series of process such as drying and machining. Ebewele (1986) studied about the effects of kiln drying and thermal degradation of wood caused by dull blades in machining on the fracture energy. The fracture energy increased with decreasing moisture content of adherends from 60 to 10%. This was because the high moisture content often led to a starved bondline where the adhesive was squeezed out by pressing during

bonding. For moisture contents below 10%, Conrad et al. (2004) mentioned in their review that the relationship between moisture content and fracture energy was similar to solid wood where the maximum fracture energy was found at approximately 6 to 8% moisture content. Heating wood at elevated temperature (250°C) can also significantly reduce the fracture energy by increasing the flaws in the bonding surface. It is important to note that in Elewele's (1980, 1986) study, aging, drying and thermal degradation of wood were all prior to bonding.

Following Elewele's studys, more effort was given to simplify the contoured DCB preparation. River et al. (1989) extended the contoured solid wood DCB to a composite specimen of wood and aluminum to overcome difficulties in the specimen preparation and testing. River and River and Okkonen (1993) replaced the aluminum with a concave-tapered specimen of oriented strand board (OSB) to overcome the difficulties in bonding and debonding between aluminum and wood. OSB can be easily removed from tested wood specimens, and re-used for additional specimens. This new composite specimen was inexpensive and allowed the wood to be bonded at a constant pressure with providing a linear relationship between compliance and crack length.

In studies by Evewele (1979), River et al. (1989), River and Okkonen's (1993), the brittle behavior of bondline was discussed. The crack-growth-rate stability index (SI) and brittle index (I) were used as follows:

$$SI = \frac{G_{Ia}}{G_{Ic}} = \frac{P_a}{P_c} \tag{7}$$

$$I = \frac{G_{Ic} - G_{Ic}}{G_{Ic}} \tag{8}$$

where G_{Ic} is fracture energy at crack initiation, G_{Ia} is fracture energy at crack arrest, P_c is force at crack initiation, P_a is crack-arrest force and u is displacement. High SI or low I indicates stable crack growth; Low SI or high I indicates catastrophic, unstable crack growth. Generally, the stable crack growth occurred in bondlines with low fracture energies, and the unstable crack growth occurred in ones with high fracture energies.

The flat DCB specimen was shown in Figure 8.

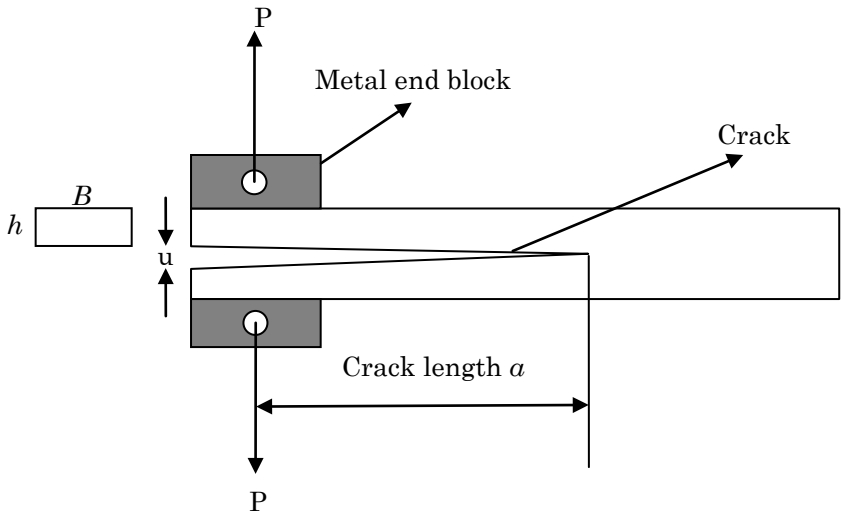

Figure 8. Flat DCB specimen under mode-I fracture

Using beam theory, the displacement, u, and compliance C were derived as follows:

$$u = \frac{2a^3P}{3EI} \tag{9}$$

$$C = \frac{8a^3}{BEh^3} \tag{10}$$

where $I=Bh^3/12$ is the second moment of area; B and h are the width and the thickness of the beam. E, the constant modulus of beam, can be found

by plotting $C^{1/3}$ against measured crack length, a. With knowledge of E, fracture energy, G_I can be directly calculated from Equation 11. Materials with relatively low beam shear modulus, such as wood, leads to rotations and deflections accruing at the crack tip. To correct this defect, Blackman et al. (1991) developed the shear correction factor, x, which can also be found from the plot of $C^{1/3}$ versus a. Therefore, the G_I was calculated as follows:

$$G_I = \frac{12P^2(a+x)^2}{B^2h^3E} \tag{11}$$

Lim et al. (1994, 1995) published the work where they used flat wood DCB specimens as shown in Figure 9. The end blocks in Figure 8 were replaced with holes drilled in the center of the beams. Also, this specimen can also be tested under mode-II and mode-III fracture, and in his study, the increasing order of $G_{Ic} < G_{IIIc} < G_{IIc}$ was determined for all adhesive joints.

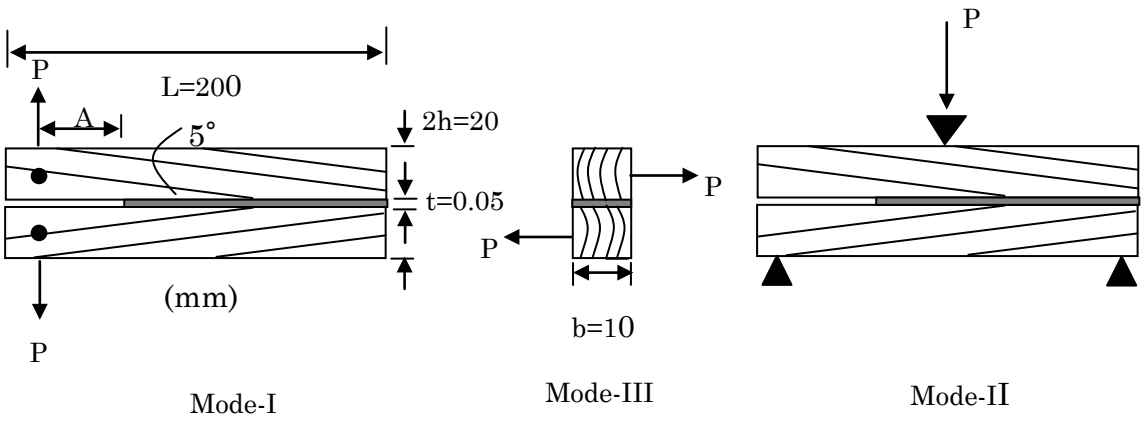

Figure 9. Flat wood DCB specimen under mode-I, mode-II and mode-III fracture

Gagliano and Frazier (2001) improved the data analysis. From Equation

9, the compliance was calculated as follows:

$$C = \frac{u}{P} = \frac{2a^3}{3EI} = ka^3 \tag{12}$$

$$C^{1/3} = k^{1/3}a = ma \tag{13}$$

where k is $2/3EI$ and m is $k^{1/3}$; m is the slope of $C^{1/3}$ versus crack length a as shown in Figure 10. Therefore, the effective stiffness, $(EI)_{eff}$, was calculated as follows:

$$(EI)_{eff} = \frac{2}{3m^3} \tag{14}$$

and Equation 11 becomes:

$$G_I = \frac{P^2(a+x)^2}{B(EI)_{eff}} \tag{15}$$

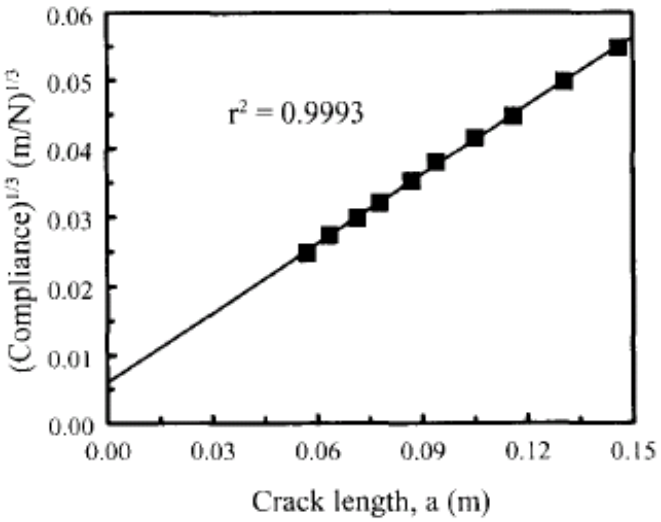

Figure 10. A typical plot of the cube root of compliance versus crack length (Gagliano and Frazier (2001))

CHAPTER THREE: INVESTIGATING THERMAL STABILITY OF WOOD ADHESIVES

3.1 INTRODUCTION

Because of fire considerations in residential buildings, more attention has recently been paid to the fire-performance and thermal stability of exterior-grade wood adhesives. Historically, most exterior-grade wood adhesives were derived from phenol/resorcinol-formaldehyde technologies; these are known for their excellent thermal stability and they have many years of demonstrated performance. Within the last 10 years, isocyanate-based adhesives and particularly polyurethane wood adhesives have entered the exterior-grade wood adhesive market. Entry into the exterior-grade market was previously based upon the rigorous "delamination test," ASTM D2559-04 (2004). However this procedure tests the adhesive resistance to extreme weathering, and no aspect of fire performance is included. Consequently, polyurethane wood adhesives successfully entered the exterior-grade market through ASTM D2559-04 (2004) qualification. Subsequently, anecdotal reports of fire-related wood-adhesive failures raised concerns across the industry; particularly since it is well known that polyurethane adhesives are less thermally stable than phenolic and resorcinolic wood adhesives. These concerns stimulated the development of new heat resistance standards; ASTM D7374-08 (2008) and D7247-07ae1 (2008) are examples. Both of these standards involve performance testing under actual fire conditions, or near wood-combustion temperatures. The focus of this research is to provide

another perspective on the thermal stability and possible fire-performance of wood adhesives. Southern yellow pine *(Pinus spp)* was bonded with resorcinol-formaldehyde or polyurethane adhesives. The thermal degradation of the bondline was tested with mode-I fracture testing under standard room conditions.

3.2 MATERIALS AND METHODS

3.2.1 Materials

Two adhesives were purchased from a local vendor: 1) A single component moisture-cure polyurethane adhesive (PUR), and 2) a two-part resorcinol formaldehyde adhesive (RF) labeled as marine grade. According to the product label, the PUR adhesive contained 100% solids. The RF solids content was measured as 73% by drying the mixed adhesive at room temperature under anhydrous N_2 and with fresh P_2O_5 for 3 days. Approximately flat-sawn, 50mm thick, southern yellow pine (*Pinus spp*.) lumber was obtained from a local vendor.

3.2.2 Dual Cantilever (DCB) Specimen Preparation

The lumber was machined into laminae with dimensions of 146 mm (tangential) X 229 mm (longitudinal) X 10 mm (radial). These laminae were machined with a grain angle of approximately 3 degrees, as measured between the longitudinal wood axis and the tangential bonding surface. The laminae were conditioned to a moisture content (MC) of approximately 12% at 20°C and 65% relative humidity. Two laminae were paired so that

the grain converged to a “V” shape at the bond-line, as observed on the radial surfaces. A 25 mm de-bond area was created using a paraffin-based marker on the specimen end exhibiting the “open” end of the V-pattern, where crack opening initiated during fracture testing.

The RF adhesive was thoroughly mixed according to manufacturer instructions and applied to one bonding surface with a hard rubber roller (adhesive coverage=214 g/m^2). The PUR adhesive was similarly applied to one bonding surface (156 g/m^2) - using a wet paper towel, the matching surface was lightly water dampened without precise measurement. The adhesive coverages were calculated and applied to achieve the same solids application. For both adhesive systems, the open assembly time was about 30 seconds; consolidation pressure was applied 10 min after closing the bonds. Eight RF and six PUR bonded laminates were consolidated (room temperature, 0.87 MPa [126psi], 24 hours). After removing about 5-8 mm from both long edges, the bonded laminates were ripped into five 20 mm wide specimens and were equilibrated under the conditions mentioned above.

3.2.3 DCB Specimen Thermal Treatment

PUR and RF DCB specimens were randomly selected and subjected to the following 5 treatments: 1) NT (control group), no thermal treatment; 2) 135C, heated at 135°C in a forced-air convection oven for 24 hours; 3) 155C, heated at 155°C, 24 hours; 4) 175C, heated at 175°C, 24 hours; 5) 200C, heated at 200°C, 24 hours. Subsequently, all specimens were equilibrated at 20°C and 65% relative humidity until the MC changed less than 0.5% per day.

3.2.4 Mode-I Fracture Testing

As needed, specimens were removed from the humidity chamber and tested in mode-I cleavage under ambient conditions using the method similar to that of Gagliano and Frazier (2001). Testing was performed on a MTS (model GL-10) 10,000 lb screw-driven test system using TestWorks 3.09 software. Immediately prior the testing, 4.3 mm dia. loading-pin holes were drilled into DCB specimens 10 mm from the specimen end containing the paraffin debond. Crack visualization was aided by coating the bondline with white typographic fluid; crack length measurement was facilitated by bonding a paper rule to the same side of the DCB. The DCB specimen was loaded in a cyclic fashion as reflected in Figure 11 Top. The crack tip was observed at approximately 10x magnification with the aid of a digital camera. Upon loading, the crack tip and load-displacement curve were simultaneously monitored; once the load peaked and the crack initiated, the crosshead displacement was fixed and held for 45 seconds. The crack naturally extended and then arrested; the arrest load and arrest crack length were recorded; and once the 45 sec period elapsed the crosshead was automatically returned to zero displacement. As measured from the loading pins, only crack lengths between 50 and 150 mm were used for fracture energy calculations. For subsequent loading cycles, the displacement rates were adjusted to achieve crack initiation within about 60 seconds from the start of loading, as described in Gagliano and Frazier (2001).

The mode-I fracture energy, G_I, was calculated as follows:

$$G_I = \frac{P_c^2 \times (a+x)^2}{B(EI)_{eff}} \tag{16}$$

Where P_c is critical load when crack extension is initiated or arrested, a is crack length, B is the DCB width, $(EI)_{eff}$ is the effective flexural rigidity of the DCB specimen, and x is a correction factor as per Blackman et al. (1991). Both $(EI)_{eff}$ and x were derived from the experimental data through the following relationships:

$$(\mathrm{EI})_{\mathrm{eff}} = \frac{2}{3\mathrm{m}^3} \qquad \mathrm{x} = \frac{\mathrm{b}}{\mathrm{m}} \tag{17}$$

where m and b are the slope and the y-intercept, respectively, from the linear trend-line of the plot of the cube root of compliance versus crack length (Figure 11, Bottom).

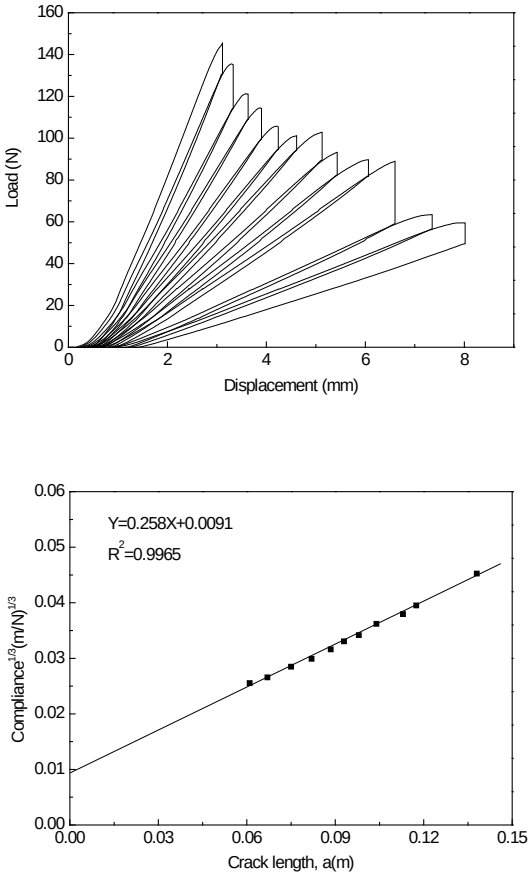

Figure 11. A typical load versus displacement curve (Top), and the corresponding plot of the cube root of compliance versus crack length (Bottom)

The squared correlation coefficient, R^2, determined from the compliance/crack length plot (Figure 11, bottom) was used to screen the suitability of fracture specimens. Specimens exhibiting an R^2 less than 0.98 were excluded from this study; as seen in Figure 12, this was 6 out of 65 specimens (9%).

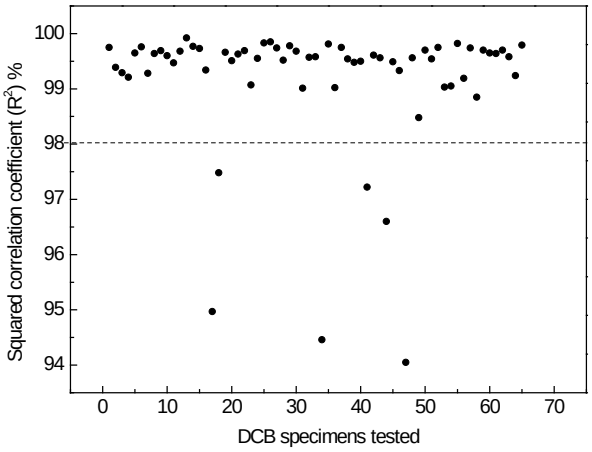

Figure 12. Squared correlation coefficients (R^2) determined from compliance/crack length plots for all DCB specimens tested in this study

On average, each DCB specimen provided about 12 cycles of crack initiation and arrest with the corresponding initiation and arrest fracture energies, respectively G_{Ic} and G_{Ia}. The number of specimens within each sample is shown in Table 1, and the total number of cycles (i.e. crack extension and crack arrest) pooled from all specimens within each sample group is shown in Table 2.

Table 1. Numbers of DCB specimens in each group

	NT	135C	155C	175C	200C
PUR	6	4	5	4	6
RF	8	8	6	8	4

Table 2. Number of fracture cycles pooled within each sample group

	NT	135C	155C	175C	200C
PUR	68	45	63	54	72
RF	106	89	70	110	50

3.2.5 Dynamic Mechanical Analysis (DMA) and Specimen Preparation

PUR and RF bonded DMA specimens were prepared using southern yellow pine flakes with dimensions of 120 mm (longitudinal) X 50 mm (radial) X 0.7 mm (tangential), and having been equilibrated to 12% MC. Using a uniform grain alignment, three-ply laminated specimens (two adhesive layers) were made using the same PUR and RF adhesive coverages previously mentioned for the fracture specimens. The RF or PUR adhesive was applied to one surface of two flakes; the third flake was sandwiched in between. In the case of the PUR bonded specimen, the center flake was lightly water dampened with a wet paper towel. Three bonded specimens were produced for each adhesive by consolidating at room temperature, 0.87 MPa (126 psi) for 24 hours. About 3 mm was removed from the perimeter of all samples, and these were subsequently cut into two different DMA specimens (14 mm X 35 mm): "L" specimens had the long dimension parallel to the longitudinal wood axis; "R" specimens had the long dimension parallel to the radial wood axis. Each bonded specimen provided 6 "L" and 3 "R" DMA specimens. Solid wood-only specimens (without adhesive) in the types of "L" and "R" were also prepared with the thickness of 1.4mm (tangential). The "L" specimen had the dimension of 35mm (longitudinal) X 10mm (radial), and the "R" specimen had the dimension of 35mm (radial) X 10mm (longitudinal). Note that the solid-wood and also the composite-wood DMA specimens were prepared from different sources of southern pine. All specimens were dried at room temperature under vacuum (5-10mm•Hg) for 24 hours over fresh P_2O_5 and then stored under anhydrous N_2 and with fresh P_2O_5. Five solid-wood "L", 5 solid-wood "R", 7 PUR "L", 4 PUR "R", 13 RF "L" and 8 RF "R" specimens were analyzed in the subsequent DMA testing.

DMA was performed on a TA instruments DMA 2980 in single cantilever bending (clamp span = 17.5mm). Specimens were clamped on the radial surface with a clamping torque of 136 N•cm, and bending occurred in the tangential direction. The limit of the linear viscoelastic region (LVR) was determined with strain sweep experiments (1Hz) at 25°C, 125°C and 200°C. Subsequent analyses were conducted within the LVR using strains of 0.03% and 0.02% for bonded and solid-wood specimens respectively. DMA experiments were conducted with sequential heating/holding/cooling segments at 1 Hz as follows: heating (25°C to 200°C, 3°C/min), isothermal (200°C, 20min), and cooling (200°C to 25°C, 3°C/min).

3.3 RESULTS AND DISCUSSION

3.3.1 Wood Specimen Moisture Content

In each group, five small pieces of wood (approximately 30mm X 30mm X 10mm) were cut from the same wood source used for DCB specimens. These small wood specimens were thermally treated in the same fashion as DCB specimens, and used to monitor the moisture content. The dry weight was obtained by heating wood at 103°C for 24 hours, and the MC was calculated as follows:

$$\mathrm{MC} = \frac{\mathrm{W_w} - \mathrm{W_d}}{\mathrm{W_d}} \times 100\% \tag{18}$$

where W_w is wet weight, and W_d is dry weight.

The MCs were approximately 12% before the thermal treatment, and dropped to values below 0% immediately after heating (-0.55% for 135C,

-0.97% for 155C, -2.61% for 175C and -8.38% for 200C specimens). Notice that negative MCs were recorded after the thermal treatment and this was likely due to mass loss associated with thermal decomposition. Consequently, final post-heating equilibrium MCs were calculated with the dry mass measured soon after the experimental thermal treatment. The equilibrium moisture contents (EMC) were recorded when the MC changed less than 0.5% per day. It was found that the EMC decreased as thermal treatment temperature increased: 11.15% for 135C, 10.65% for 155C, 8.95% for 175C and 7.25% for 200C specimens respectively. This thermally induced reduction in wood EMC was consistent with the results of Tjeerdsma, Boonstra etc. (1998) and Akyildiz, Ates (2008).

3.3.2 Modulus of Elastic E (MOE) of Wood

The flexural rigidity, *EI*, of the wood beams was determined experimentally as described above (Equation 17), and the second moment of area, *I*, was calculated as follows:

$$\mathrm{I} = \frac{\mathrm{Bh}^3}{12} \tag{19}$$

where *B* and *h* are the width and thickness of a single wood beam. Therefore, *E* was obtained by dividing Equation 17 (left) with Equation 19; the mean *E* values for all tested DCB are presented in Figure 13. Notice that in fracture testing, two wood beams that made up the DCB specimen were assumed to have the same elastic modulus, and the *E* obtained above is the effective modulus of these two beams rather than the modulus of either single beam. The *E* at NT, 135C, 155C and 175C has no statistically

significant difference. This was expected, because the effect of temperature at this range on elastic modulus is minimal. The *E* at 200C is significantly lower than NT, 135C and 155C groups, but not significantly different from 175C group. This can be explained by that some chemical bonds in wood begin to break down at about 175°C, and the thermal degradation of hemicellulose and lignin begins at about 200°C.

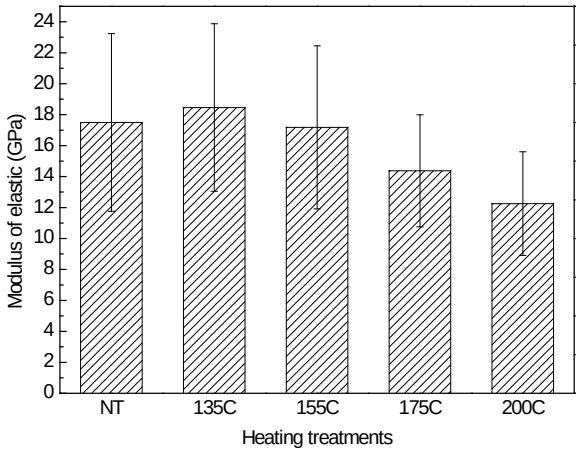

Figure 13. Effective elastic modulus of two wood beams. Error bars indicate plus or minus one standard deviation.

The thermally induced modulus reduction does not negatively impact the fracture testing results; this is because the energy calculation for each DCB is based upon its unique modulus, and this is measured for each specimen as described above (Figure 11, bottom).

3.3.3 Mode-I Fracture Testing

The critical and arrest fracture energies of PUR and RF bonded specimens were obtained following section 3.2.4. Within each sample group, the distribution of fracture energies was tested for normality; only the data for RF-155C was found to be non-Gaussian. Treatment effects were

analyzed both with simple non-paired t-tests (assuming normality) and also with the non-parametric Mann-Whitney test (non-normal). The results were independent of the statistical method and so the following discussion reflects simple t-testing; the criterion for statistical significance was assigned as $p \leq 0.05$.

Within the control group (NT) as shown in Figure 14, PUR exhibited significantly higher fracture toughness than RF, as expected from the known differences in crosslink density for the two adhesives. The heating treatment significantly decreased the fracture toughness of both PUR and RF bonded specimens. Recall that all specimens were tested at room temperature after moisture equilibration, and so Figure 14 reflects irreversible thermal degradation and not simple thermal softening of wood or adhesive. Also for both adhesives, increasing heating temperatures significantly reduced fracture energies with respect to the next lower treatment temperature; an exception was noted for the arrest fracture energies of PUR-135 and RF-155C which were not significantly lower than for specimens treated at the next lower temperature. Figure 14 also shows that PUR bonded specimens tended to exhibit greater fracture toughness variation; but the toughness distributions narrowed significantly for both adhesives after the two highest thermal treatments.

About the fracture energy of pure wood at high temperature, Reiterer (2001) tested the spruce and beech immediately after the heating up to 80°C, and found that their toughness decreased as a function of temperature. Although there is no direct report about the nonreversible toughness change of wood at the temperature range we tested, it is possible that the reduction of wood toughness due to thermal degradation was also involved during the fracture testing.

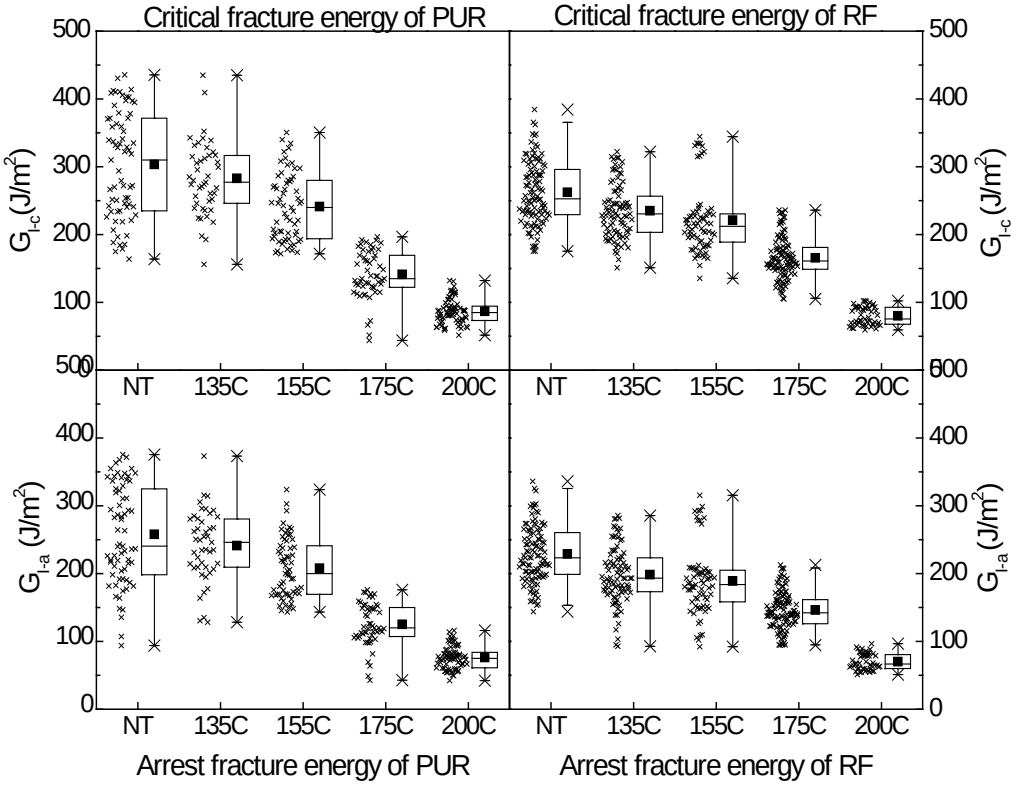

Figure 14. Critical (Top) and arrest (Bottom) fracture energies of PUR (Left) and RF (Right); Symbols as follows: maximum/minimum (X), 1st and 99th percentile (whiskers), 25th and 75th percentile (box), and the arithmetic mean (black square).

The thermally induced decline in fracture toughness is depicted again in Figure 15. While PUR specimens started with a higher toughness, the percentage decline in toughness was comparable for PUR and RF up to the 155˚C treatment temperature; at higher temperatures the percentage reduction in toughness was significantly greater in PUR specimens. Interestingly however, after the highest temperature treatment both sample types exhibited about the same toughness.

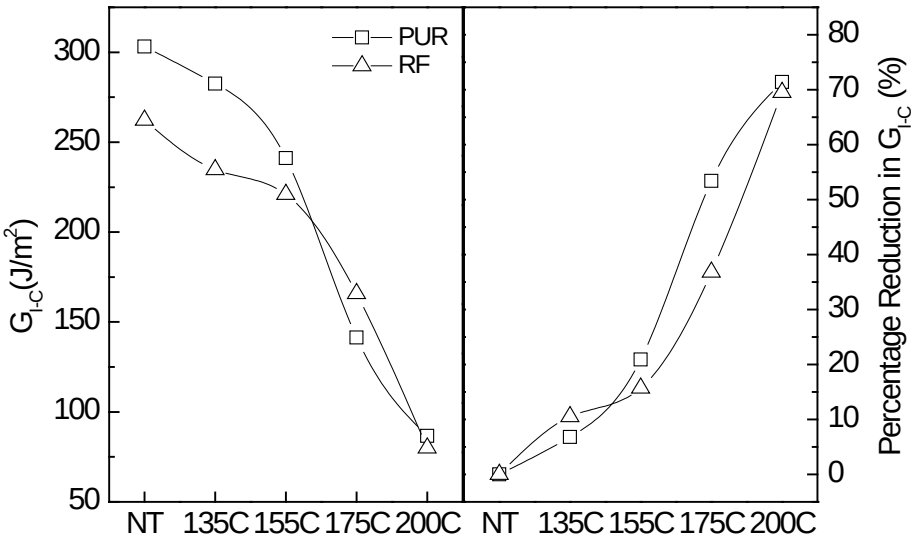

Figure 15. The average critical fracture energies (Left) of PUR and RF. Percentage reduction in critical fracture energy (Right)

3.3.4 DMA Testing

In an effort to gain more insight about the effects of the thermal treatment on fracture specimens, solid-wood and bonded specimens were subjected to DMA during which specimens were heated to 200°C, and then held at this temperature for 20 minutes prior to subsequent cooling. Figure 16 shows the dynamic thermal scans of solid-wood specimens as a function of analysis time; the corresponding temperature profile is also indicated.

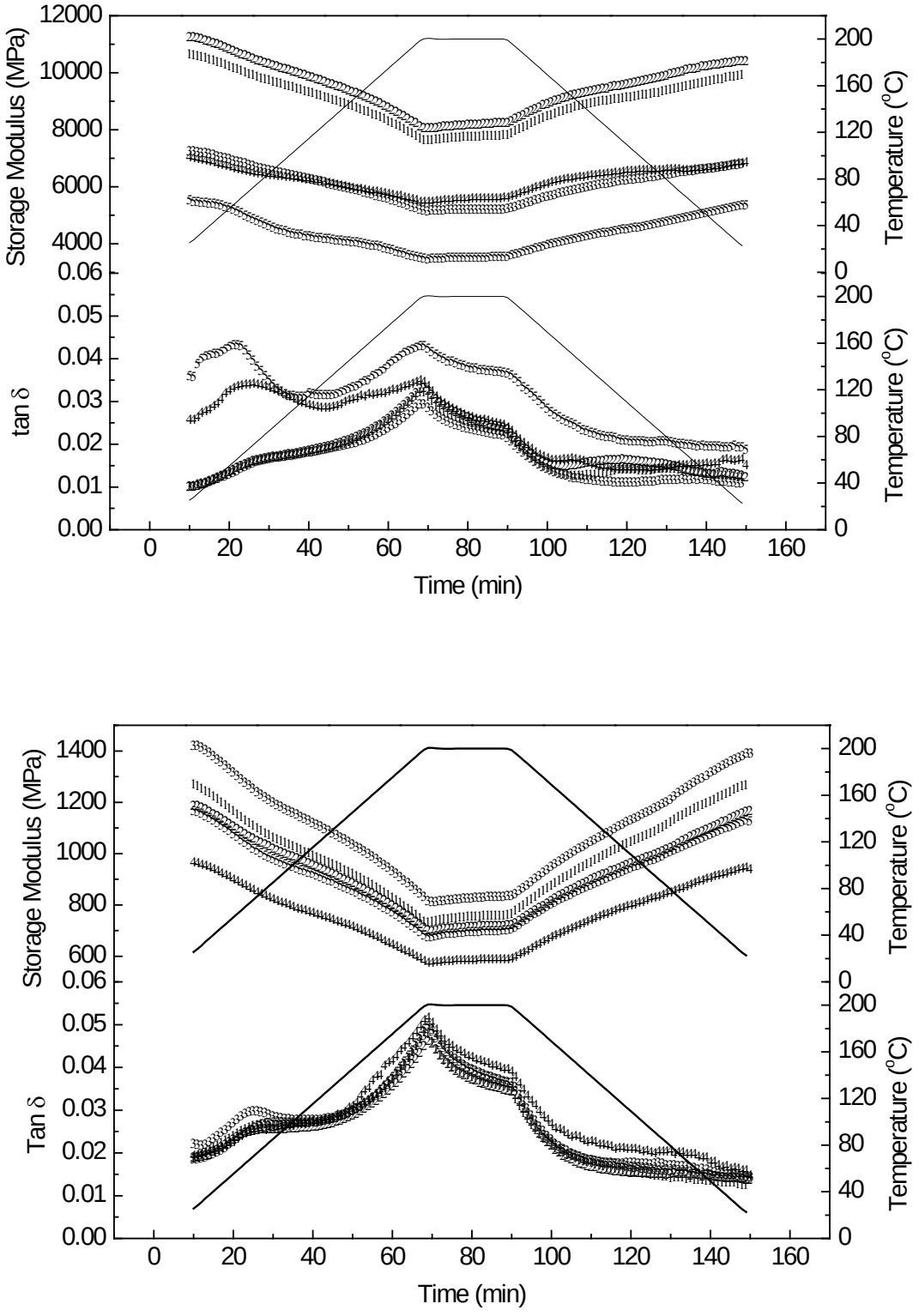

Figure 16. Storage Modulus and tan δ of solid-wood "L" (top) and solid-wood "R" (Bottom) specimens. Five specimens for each group

As expected, the storage modulus of solid-wood "L" specimens was about 10 times greater than for solid-wood "R" specimens. During heating, the storage modulus of all solid-wood specimens exhibited a relatively minor decrease that is characteristic of dry wood over this temperature range; during the high temperature isothermal heating a very minor stiffening was observed, which might be due to thermally induced crosslinking and/or increases in cellulose crystallinity; upon cooling the storage modulus returned nearly to the original level seen prior to heating. As for the tan δ response, solid-wood "R" specimens exhibited a more uniform behavior than was seen in the "L" specimens; and characteristic of the cross-grained response, "R" specimens exhibited slightly greater damping intensities than did the "L" specimens. Although somewhat variable, the tan δ response generally increased during the heating phase, and this was accompanied by a minor damping peak at approximately 40 to 50°C; during the high temperature isothermal heating the tan δ response exhibited a rather steep decline; upon cooling the tan δ response declined sharply and then leveled to a nearly flat response. The responses observed in Figure 16 reflect the complex structure of wood in which oriented cellulose fibrils are embedded within an amorphous lignin matrix, and where non-cellulosic polysaccharides (glucomannans and xylans) are believed to associate specifically with cellulose and/or lignin. No attempts were taken to associate specific relaxations with wood-polymer structural features. However, since the specimens were dry it is certain that no major segmental relaxations (such as a glass transition) were observed. Instead, the responses seen in Figure 16 are very weak and are probably characteristic of secondary relaxations and perhaps also interactions between different wood polymers.

Figure 17 shows the dynamic thermal scans of PUR composite specimens. The storage modulus of the PUR composite specimens was significantly lower than was noted for the solid-wood specimens above. The reason for this difference is unknown, and could simply reflect the different wood sources for the composite and solid-wood specimens respectively. Overall, the DMA response of the PUR specimens was similar to that seen for the solid-wood specimens. One notable difference was seen from three PUR "L" specimens that exhibited a substantial tan δ increase starting near 120°C. Furthermore, upon reaching 200°C the PUR specimens exhibited a greater softening than was seen in the solid-wood specimens; and after complete cooling, the PUR specimens recovered less of the original stiffness seen prior to heating. The discussion will return to these points later.

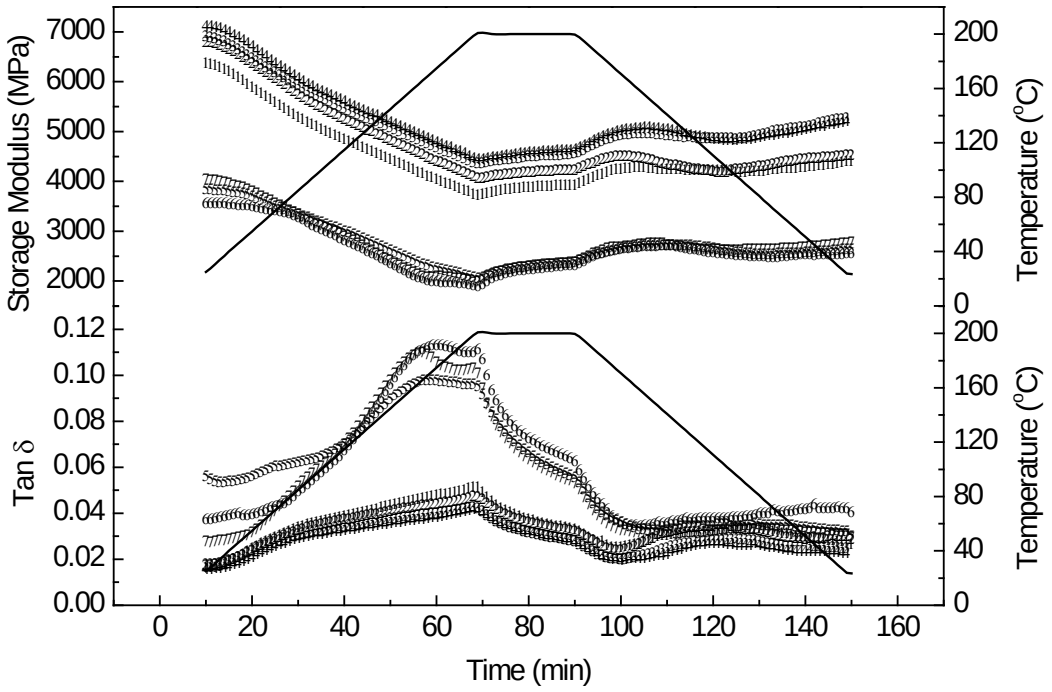

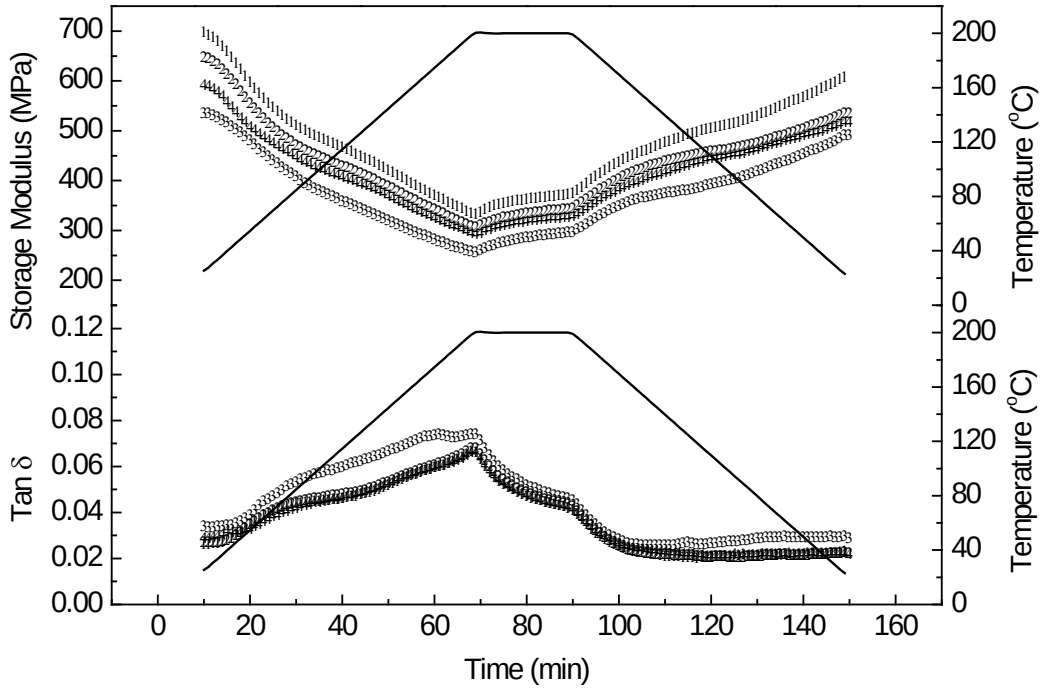

Figure 17. Storage Modulus and Tan δ of PUR "L" (Top) and PUR "R" (Bottom) specimens. 7 PUR "L" and 4 "R" specimens were analyzed and presented.

With respect to the RF-bonded DMA specimens, the most notable feature was that DMA scans within this sample exhibited a great deal of variability. Figure 18 presents the DMA scans for RF "R" specimens, where the top panel displays the responses that were most uniform, and that appeared most similar to the solid-wood and PUR specimens previously discussed; the bottom panel displays the more variable specimens where a more complex response is seen, characterized by multiple peaks in the tan δ response. The cause of the more variable and complex response (in comparison to the solid-wood and PUR specimens) is unknown; however this could be related to excessive crosslinking and bondline embrittlement that could be expected from the high crosslink density RF adhesive.

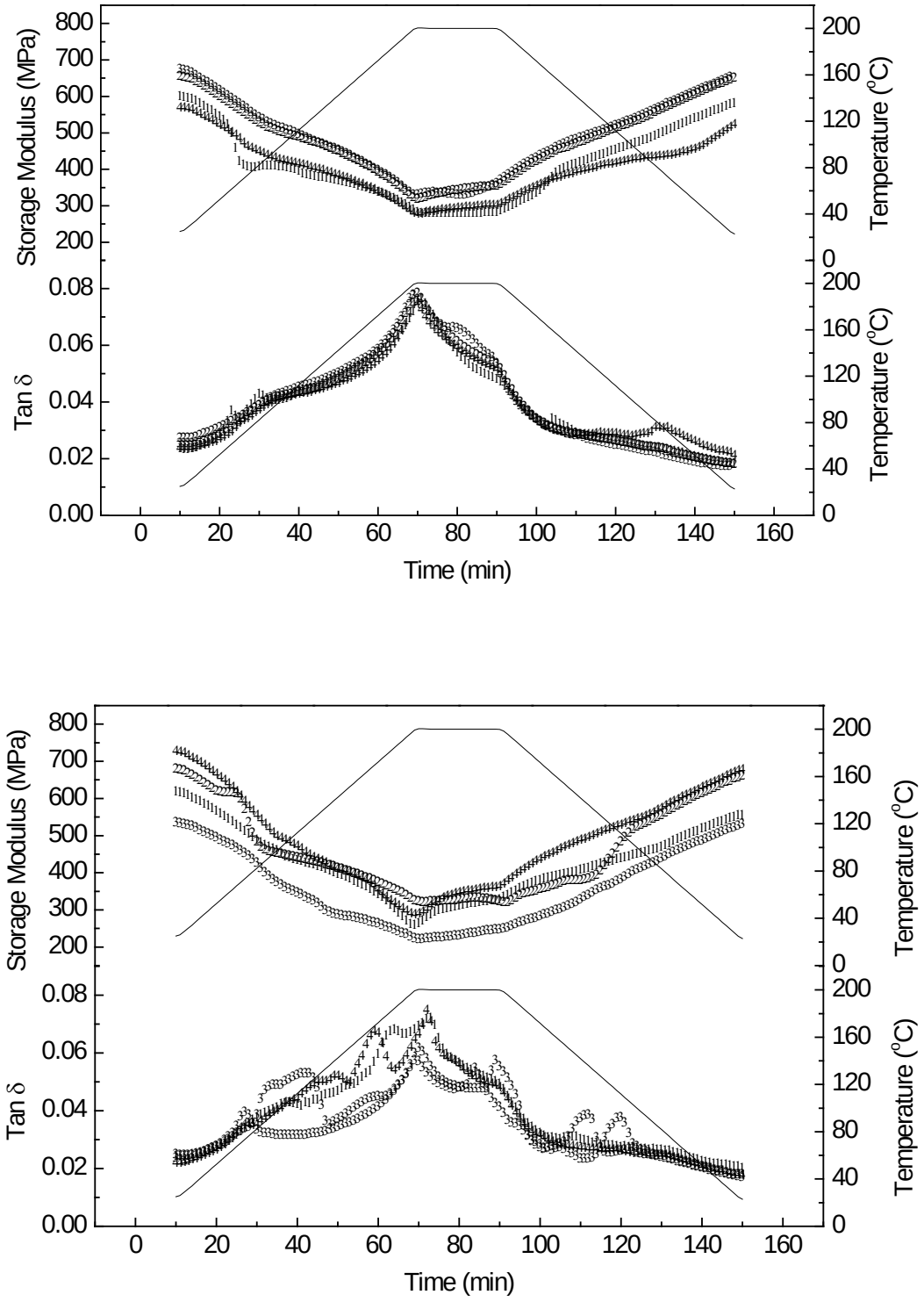

Figure 18. Storage Modulus and Tan δ of 4 RF "R" specimens having reproducible behavior (Top) and 4 RF "R" specimens having non-reproducible behaviors (Bottom). Total 8 specimens were analyzed and presented.

The RF "L" specimens were even more variable and complex than the RF "R" specimens; Figure 19 presents four randomly selected RF "L" scans that are provided simply to demonstrate the general response.

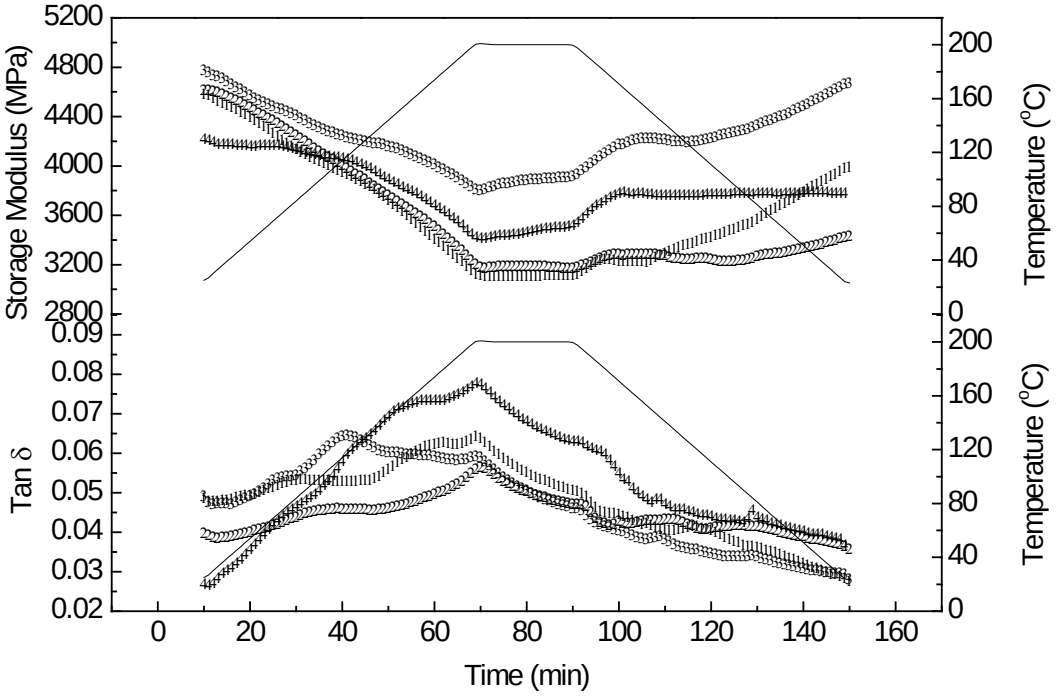

Figure 19. Storage modulus and Tan δ of RF "L" specimens. Thirteen specimens were analyzed, and 4 of them were randomly selected and presented.

Percentage decreases in the storage moduli upon heating to 200°C (200C) and after cooling (post-cooling) are shown in Figure 20. In general, three differences between "R" and "L" specimens are observed: "R" specimens show a greater percentage modulus decrease upon reaching 200C: "R" has a lower percentage decrease at post-cooling; "L" specimens exhibit greater variability. The cause of these differences could be different wood grain orientations in the two types of specimen.

As for solid-wood specimens, decreases of about 28% ("L") and 42% ("R")

in storage moduli are observed for the 200C, and the storage moduli recovered when cooled. At post-cooling, the percentage decrease for solid-wood specimens was reduced to about 5% (“L”) and 2% (“R”).

It was observed that the percentage decreases in the composite specimens were greater than in the solid-wood specimen except that for the 200C, the difference between solid-wood and “L”-RF is not significant. For the 200C, the differences of the percentage decrease between composite specimens and solid-wood specimen were due to the thermal softening and/or the thermal degradation of the adhesives upon heating to 200°C. At post-cooling, these differences were attributed to the irreversible thermal degradation of adhesives after cooling.

As for “R” specimens, for the 200C, the difference of the percentage decrease between solid-wood and PUR is at the same level as the difference between solid-wood and RF. Thus, the degrees of thermal softening and thermal degradation for PUR and RF upon heating to 200°C are similar. After cooling, the difference of percentage decrease between solid-wood and RF was reduced, while the difference between solid-wood and PUR remained same. Thus, in heating to 200°C, RF has more reversible thermal softening than PUR does.

As for “L” specimens, for the 200C, PUR’s percentage decrease was significantly greater than solid-wood, but the difference between solid-wood and RF is not significant. Thus, the RF did not show significant thermal softening or thermal degradation upon heating to 200°C, while PUR did. After cooling, the difference was increased for both PUR and RF. Thus, there was some thermal degradation during cooling, which can not be explained.

In the single cantilever bending, the transverse shear stress along the

longitudinal axes of the specimen is developed from the vertical shear stress. More details are summarized in Appendix A. Because the tensile stiffness of the cellulose fibrils along the longitudinal direction (L specimen) is greater than the one of the cellulose fibrils along the radial direction (R specimen), L specimen has greater bending stiffness than R specimen. To achieve the same bending strain, more shear stress is applied to L specimen, so the transverse shear stress in the adhesive layer in L specimens is greater than in R specimens. This high shear stress in the bondline may be the reason why L behaves differently from R, and has significantly higher variations.

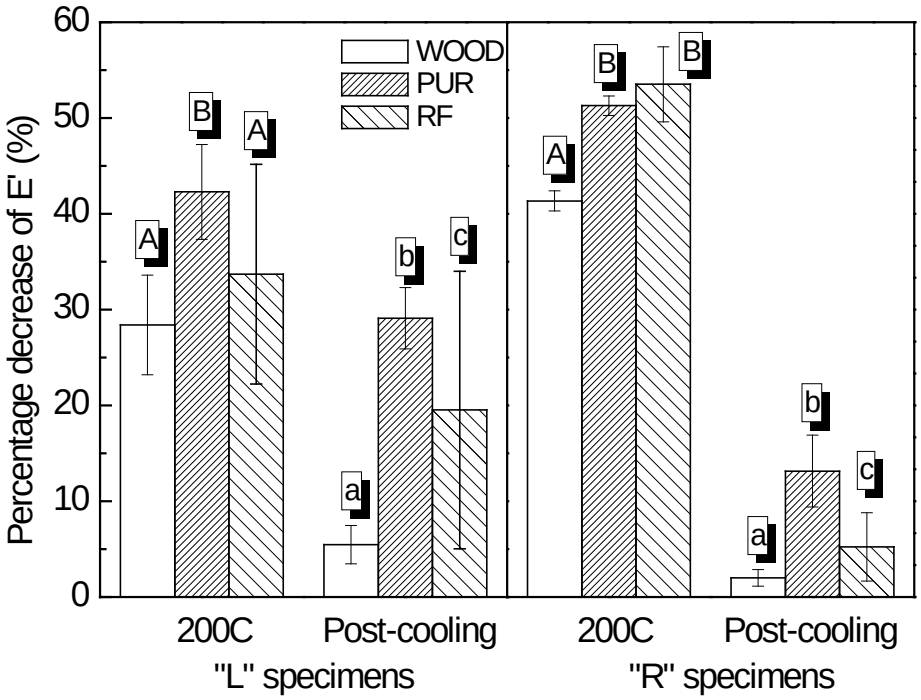

Figure 20. The percentage decrease in the storage moduli upon heating to 200°C (200C) and after cooling to the starting temperature (Post-cooling); based upon the initial storage modulus prior to heating. Same letter above the column indicates non-significant difference.

3.4 CONCLUSIONS

The fracture testing result shows that the PUR is tougher than the RF at room condition, and both adhesives were thermally degraded after thermal treatment. DMA result suggested that the toughness loss in the PUR is simply because of the excessive thermal softening and/or thermal degradation at high temperature. Therefore, the PUR should be modified to improve its thermal resistance at high temperature, consequently to improve its fracture performance.

CHAPTER FOUR: EFFECTS OF THERMAL DEACTIVATIO OF WOOD ON WOOD/PE ADHESION

4.1 INTRODUCTION

Within the last 20 years, composite materials made from wood particles and common thermoplastic polymers have grown to occupy a significant portion of the home construction market. Such wood/thermoplastic composites are principally used for home decking and railing applications. A variety of thermoplastic polymers are used, such as poly(vinylchloride), poly(styrene), and poly(propylene); poly(ethylene), PE, is perhaps the most common. Generally, the natural fiber used in these materials is selected according to the proximity of the source since transportation costs are often a limiting factor. Wood/thermoplastic composites are necessarily low cost and narrow profit margin materials. Consequently, there is little opportunity to employ interfacial coupling agents that neutralize the dramatic polarity difference between wood and PE. Recently, Follrich et al. (2006) demonstrated that adhesion between spruce (*Picea abies Karst*.) wood and PE was significantly improved if the wood was surface deactivated by heat treatment. The contention in this work was that wood-surface thermal deactivation could serve as a relatively simple surface treatment to improve the performance of wood/thermoplastic composites. While wood thermal deactivation might be simple, it does incur a significant energy cost, and so even this process could prove to be cost prohibitive. However other developments in the forest products industry

could perhaps improve the economics of using thermally deactivated wood particles. Recently, thermally modified wood building elements (dimension lumber) have been introduced into the European and North American markets. These materials are heat treated past the point of significant thermal degradation. Such heat treatments are thought to destroy the very hydrophilic non-cellulosic polysaccharides in wood; these are the glucomannans and xylans which collectively are referred to as "hemicellulose." Such extreme thermal degradation transforms wood into a hydrophobic material that is decay resistant and dimensionally stable to moisture changes (Del Menezzi, et al., 2005, 2008); and while the strength also decreases, wood stiffness is reduced to a minor degree or perhaps not at all depending upon the severity of the treatment. When properly prepared, thermally modified wood building elements can be effectively employed also as decking and railing materials. This strategy of hydrophobic transformation could be adopted by other wood industries that commonly work against the moisture-related dimensional instability of wood. Such technological developments might then improve the economics of using thermally deactivated wood particles in wood/thermoplastic composites. Within this context, the present study was directed towards the adhesion of PE to thermally deactivated southern yellow pine (*Pinus spp*.) As in the work of Follrich et al. (2006), adhesion was studied using mode-I fracture.

4.2 MATERIALS AND METHODS

4.2.1 Materials

Southern yellow pine (*Pinus spp.*) lumber, approximately flat-sawn (thickness = 50mm) was obtained from a local vendor. Low density polyethylene (LDPE) film (density=0.92g/cm^3, thickness=0.05mm) was purchased from Goodfellow, US.

4.2.2 Melting Temperature of LDPE

To determine the flow properties of the LDPE, parallel-plate dynamic mechanical analysis was conducted using a TA instruments AR1000 equipped with 25mm dia. disposable plates. Two layers of LDPE film were stacked and tested in the following 4 steps with the oscillation frequency of 1Hz: (1) heating (40°C to 110°C, 3°C/min), normal force=5N, stress=400Pa; (2) heating (110°C to 200°C, 3°C/min), normal force=0N, stress=100Pa; (3) cooling (200°C to 100°C, 3°C/min), normal force=0.1N, stress=100Pa; (4) cooling (100°C to 40°C, 3°C/min), N=0.1N, stress=400Pa.

4.2.3 Thermal Modification (TM) of Wood Bonding Surfaces

Lumber was machined into 24 laminae, 175mm (Tangential) X 225mm (Longitudinal) X 13mm (Radial) and a grain angle (measured between the longitudinal wood axis and the tangential bonding surface) of approximately 3 degrees. The laminae were dried in an oven to a moisture content of approximately 2% at 55°C for about 48 hours; this caused minor specimen cupping. Samples were planed to a final thickness of 10mm,

which removed any cupping. Small specimens for contact angle (CA) measurements were sawn as illustrated in Figure 21. Laminae and CA specimens were paired and closed to protect the freshly machined bonding surfaces, and subsequently sealed in plastic bags to prevent moisture uptake during storage.

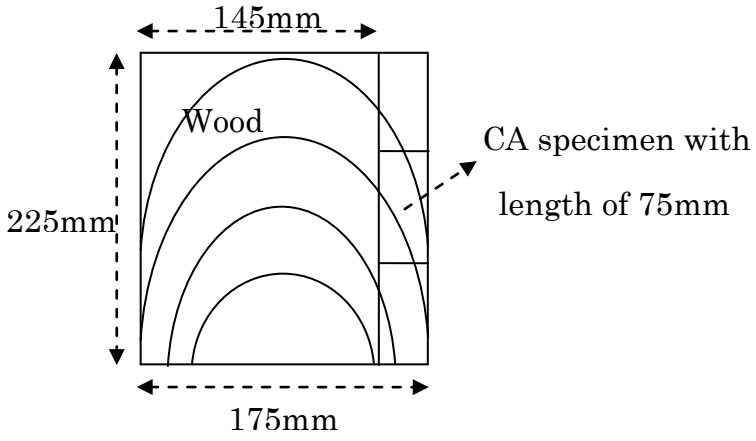

Figure 21. Wood lamina for bonding and specimens for contact angle (CA) measurement.

The dried laminae and CA specimens were randomly divided into 4 groups (6 laminae and 18 CA specimens in each group). One control group received no further treatment (NOTR), and the other three groups were heated at 180°C for 5min (TM5), 15min (TM15), and 60min (TM60) respectively. During heating, laminae and CA specimens were placed in the oven with machined surfaces exposed, and timing began once the temperature inside the oven reached 180°C. After heating, samples were cooled under anhydrous conditions (dessicator with N_2 gas and P_2O_5); laminae were then stored in plastic bags and the CA specimens remained in the desiccator for storage. The laminae and CA specimens in the NOTR group were stored in the same manor as TM groups.

4.2.4 Contact Angle Measurement

The contact angle was measured with FTA 200 Dynamic Contact Angle Analyzer using de-ionized water (droplet volume ~8ul). CA samples were taken from the desiccator immediately prior to analysis and oriented with longitudinal axis perpendicular to the camera and with the machined surface up. Images were recorded every 0.033 seconds, and contact angles were measured from the images corresponding to 0.2 seconds after droplet contact. Mean contact angles determined from both sides of the droplet were recorded. Two measurements (one on early wood and one on late wood) were taken on each CA specimen.

4.2.5 Duel Cantilever Beam (DCB) Specimen Preparation

Two laminae were paired so that the grain converged to a "V" shape at the bond-line, as observed on the radial surfaces. The LDPE film was cut to 150mm X 230mm, and sandwiched between the laminae. The assembly was hotpressed for 25min under pressure of 1.52MPa [220psi] and core temperature of 170°C. Immediately after that, the assembly was removed from the hotpress and then allowed to cool under pressure of 0.86MPa [125psi]. After removing about 5-8 mm from both long edges, the bonded laminates were ripped into five 20 mm wide DCB specimens. Within each group, DCB specimens were categorized by the grain pattern and location from where they were cut from the original laminate as shown in Figure 22. To avoid grain pattern effects one type-3 DCB specimen was removed, and seven (three type-1, three type-2 and one type-3) DCB specimens were selected for simulated weathering (W). The simulated weathering involved submerging specimens in tap water for 2 minutes followed by drying at

55°C overnight. The four weathered groups were named as NOTRW, TM5W, TM15W and TM60W. The numbers of specimens and total fracture cycles are shown in Table 3. Two NOTRW specimens de-bonded as a result of weathering and were subsequently removed, and one NOTRW specimen was removed because of relatively lower suitability. All weathered and un-weathered DCB specimens were stored in individual plastic bags until testing.

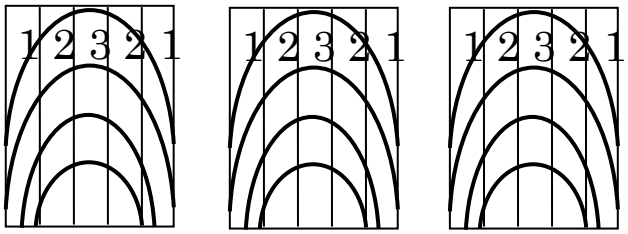

Figure 22. Selecting and regrouping DCB specimens. Each group had 15 specimens from three assemblies. Type-1: the first DCB from the edge; type-2: the second DCB from the edge; type-3: the DCB in the center.

Table 3. Numbers of specimens and total fracture cycles for each group

Un-weathered	NOTR	TM5	TM15	TM60
Specimens	7	7	7	7
Fracture cycles	96	88	83	79
Weathered	NOTRW	TM5W	TM15W	TM60W
Specimens	4	7	7	7
Fracture cycles	44	66	76	90

4.2.6 Three-Point Bending Testing

After fracture testing, debonded specimens were subjected to three-point bending in order to obtain the stiffness of the individual de-bonded wood beams as depicted in Figure 23. The beams were supported with a 200mm span (AB); loading (*P)* was applied at a rate of 0.25 mm/min at the center C of the span. The crosshead was manually stopped at crosshead displacement of d=2 mm. The stiffness, *EI*, was calculated as follows:

$$EI = \frac{\mathrm{P}}{\mathrm{d}}\frac{\mathrm{L}^3}{48} \tag{19}$$

where E and I are the elastic modulus and second moment of area respectively; L is the length of span AB. The P/d was obtained from the slope of the loading curve as shown in Figure 24.

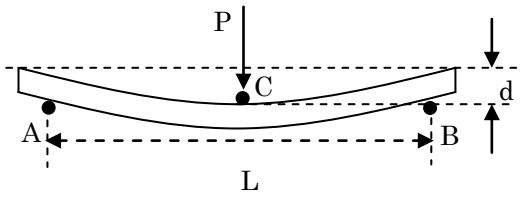

Figure 23. Three-point bending testing

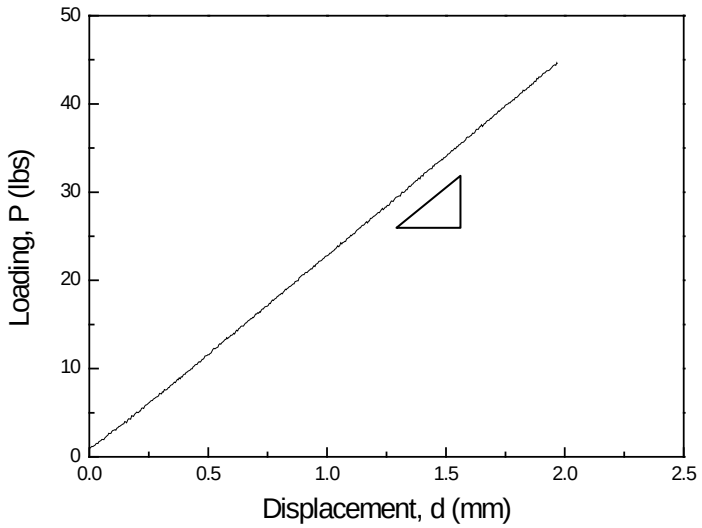

Figure 24. Typical loading versus displacement curve in three-point bending testing

4.2.7 Mode-I Fracture Testing

As needed, specimens were removed from the plastic bags and tested in mode I cleavage under ambient conditions using the method similar to that

of Gagliano and Frazier (2001). Testing was performed on a MTS (model GL-10) 10,000 lb screw-driven test system using TestWorks 4.10 software. Immediately prior testing, 4.3 mm dia. loading-pin holes were drilled into DCB specimens 10 mm from the specimen end (open side of the "V"). Crack visualization was aided by coating the bondline with white typographic fluid; crack length measurement was facilitated by bonding a metric paper-rule to the same side of the DCB. The DCB specimen was loaded in a cyclic fashion as seen in Figure 25, top. The crack tip was observed at approximately 10x magnification with the aid of a digital camera system. A 5N preload was applied to avoid an initial noisy signal. Upon loading, the crack tip and load-displacement curve were simultaneously monitored; once the load peaked and the crack initiated, the crosshead displacement was fixed and held for 45 seconds. The crack naturally extended and then arrested; the arrest load and arrest crack length were recorded; once the 45 sec period elapsed the crosshead was automatically returned to zero displacement. As measured from the loading pins, only crack lengths between 50 and 150 mm were used for fracture energy calculations. For subsequent loading cycles, the displacement rates were adjusted to achieve crack initiation within about 60 seconds from the start of loading, as described in Gagliano and Frazier (2001).

The mode-I fracture energy, G_I, was calculated by Equation 20 and 21.

$$G_I = \frac{P_c^2 (a+x)^2}{B(EI)_{eff}} \tag{20}$$

where P_c is critical load when crack extension is initiated or arrested, a is crack length, B is the DCB width, $(EI)_{eff}$ is the effective flexural rigidity of the DCB specimen, and x is a correction factor as per Blackman et al.

(1991). Both $(EI)_{eff}$ and x were derived from the experimental data through the following relationships:

$$(\mathrm{EI})_{\mathrm{eff}} = \frac{2}{3\mathrm{m}^3} \qquad \mathrm{x} = \frac{\mathrm{b}}{\mathrm{m}} \tag{21}$$

where m and b in Equation 21 are the slope and the y-intercept respectively from the linear trend-line of the plot of the cube root of compliance versus crack length (Figure 25, Bottom). Two linear regions were found at the initial and the end of each loading curve as shown in Figure 26. The compliance was taken from the initial linear region. The reason why the initial linear region was used will be discussed in section 4.3.3.

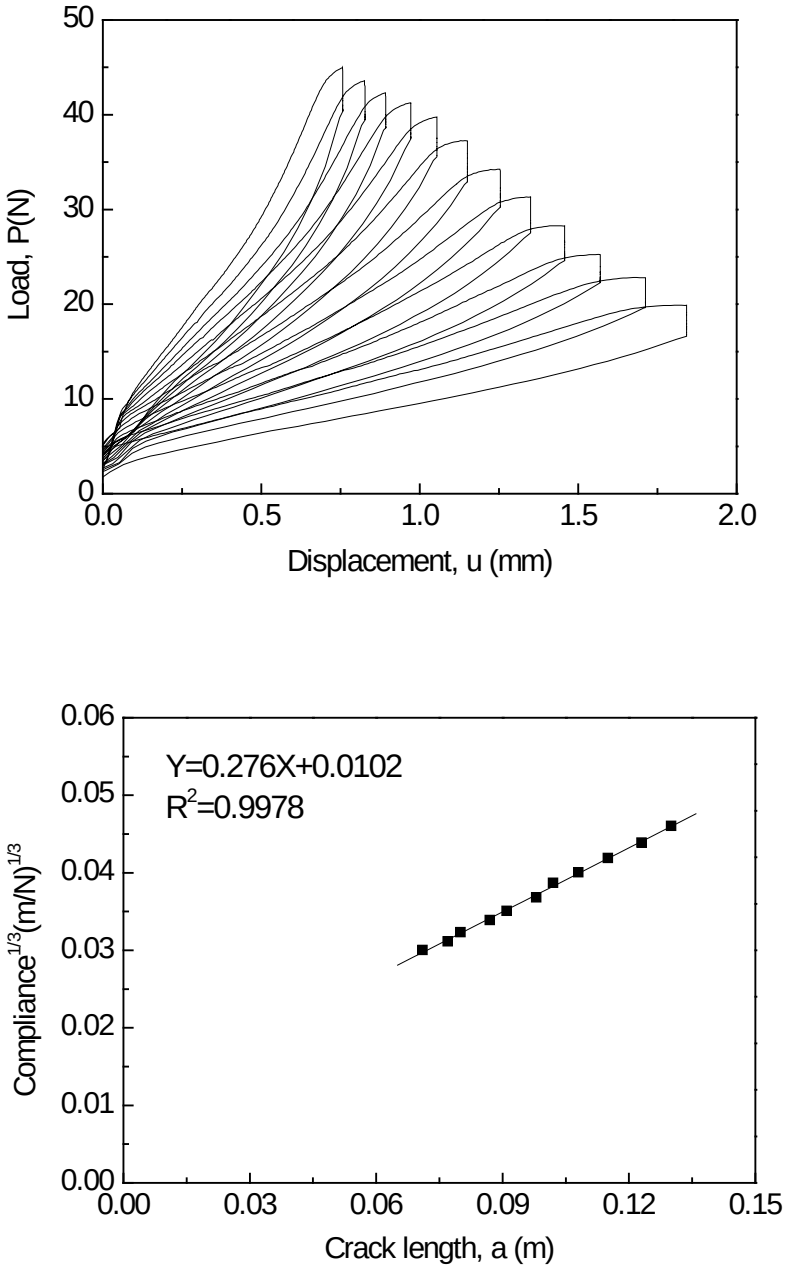

Figure 25. A typical load versus displacement curve (Top); the corresponding plot of the cube root of compliance versus crack length (Bottom).

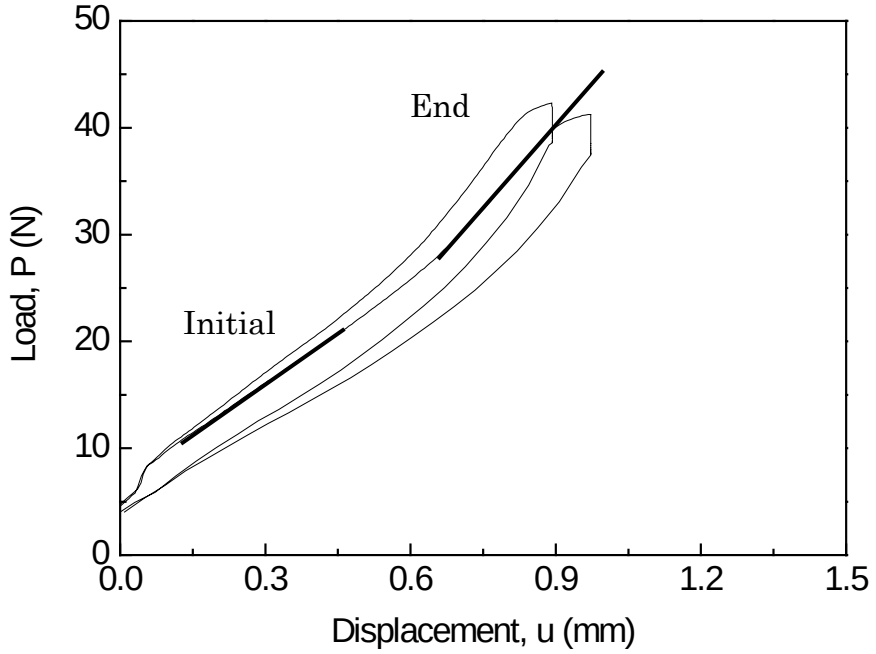

Figure 26. Two loading cycles from Figure 25 (Top). Two linear regions were found in the initial and the end of each cycle.

4.3 RESULTS AND DISCUSSION

4.3.1 Melting Temperature of LDPE

As shown in Figure 27, the melting temperature of the LDPE was determined to be approximately 110°C Beyond melting, G' decreased gradually. From this data it was determined that a DCB core temperature of 170C should be obtained during specimen hotpressing; this was intended to promote wood penetration, although penetration was not investigated.

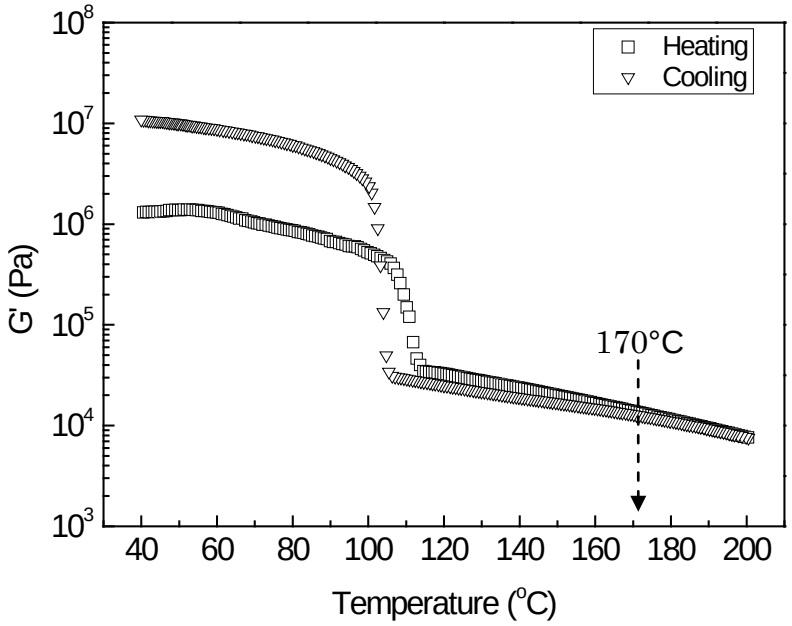

Figure 27. Storage modulus heating and cooling curves of the of the LDPE film used in this study. Vertical dashed line indicates the core temperature (170°C) achieved during hotpressing.

4.3.2 Thermal Deactivation of Wood Surfaces

Figure 28 demonstrates that wood surface energy declined as the specimen heating time increased; the water contact angle increased. Control specimens showed no clear difference in the surface energies of earlywood and latewood. As heating time increased, the earlywood appeared to be more sensitive to thermal deactivation. Aside from the earlywood/latewood effects, the results from Follrich et al. (2006) were similar.

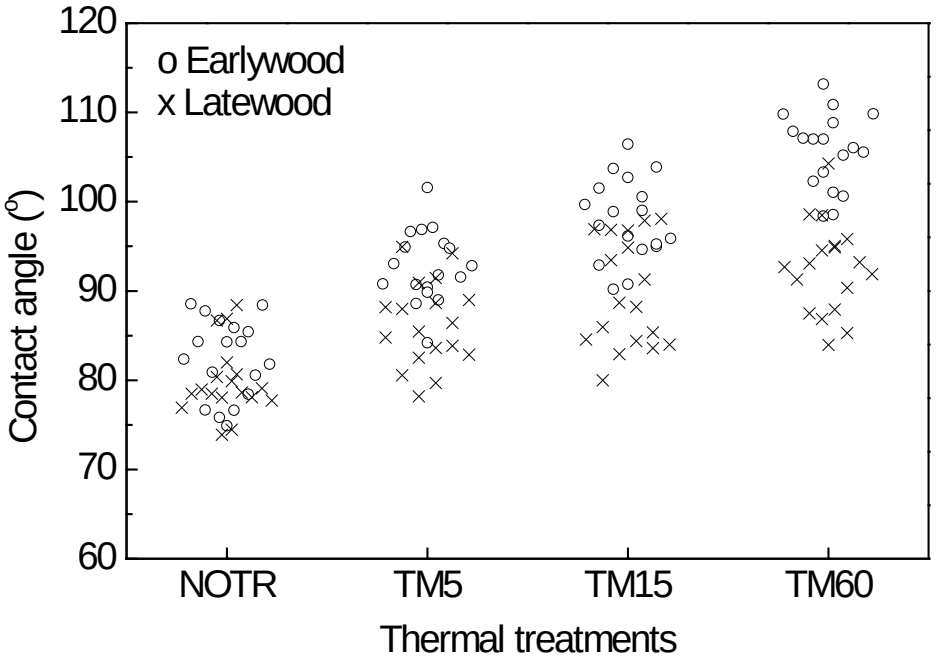

Figure 28. Water contact angles on wood surfaces at different thermal treatments

4.3.3 Nonlinear Loading Curve in Fracture Testing.

As shown in figures 25 and 26, LDPE bonded DCB's exhibited a complex nonlinear loading curve. This nonlinear response was not reported in the work of Follrich et al. (2006). Close inspection of Figure 26 reveals two roughly linear regions separated by an upward curving nonlinear response. This behavior clearly invalidated the linear elastic data treatment used in equations 20 and 21. A rigorous nonlinear data treatment was considered to be too laborious. While erroneous, the linear analysis and associated error was accepted for simplicity, and with the intention of obtaining a simple comparative analysis within this study. Nevertheless, it was necessary to determine which portion of the loading curves should be used for the linear analysis. A study was devised such that individual beams (taken from tested/debonded DCB's) were tested in three-point bending to

determine the actual stiffness (compliance). Bending tests were conducted on 14 single beams from 7 DCB specimens as described in 4.2.6. Each DCB specimen consists of two wood beams, beam-1 and beam-2, with respective effective stiffnesses, $(EI)_1$ and $(EI)_2$. From fracture testing, it was assumed that beam-1 and beam-2 have same stiffness, $(EI)_{eff}$, calculated using the compliance method. Correspondingly, $(EI)_{12}$, the harmonic mean of $(EI)_1$ and $(EI)_2$ was introduced as follows:

$$\frac{2}{(EI)_{12}} = \frac{1}{(EI)_1} + \frac{1}{(EI)_2} \tag{22}$$

Furthermore, obtained from the DCB loading curves were compliance values from the two roughly linear response regions. Figure 29 shows $(EI)_{12}$ and $(EI)_{eff}$ values derived from the initial and subsequent linear regions. Both $(EI)_{eff}$ values are close to the $(EI)_{12}$, and it is difficult to determine which one is closer. In other words, either the initial slopes or the end slopes can be used to derive the effective stiffness.

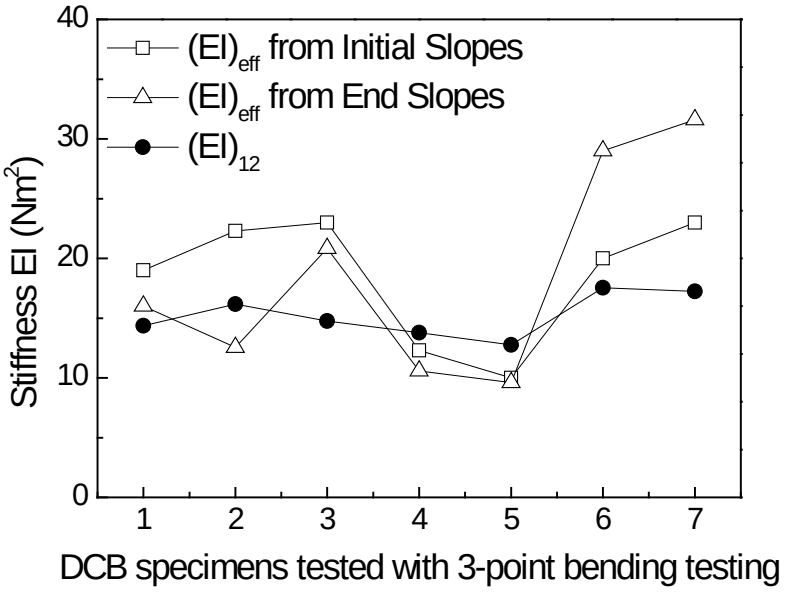

Figure 29. Comparing $(EI)_{12}$ and $(EI)_{eff}$ derived from initial slopes and end slopes. $(EI)_{12}$ was calculated from $(EI)_1$ and $(EI)_2$

To further investigate the nature of the complex DCB loading curves, a fractured DCB specimen was clamped and loaded as shown in Figure 30. The relationship between loading P and displacement u was found to be perfectly linear, implying that the nonlinear behavior was due to the LDPE adhesive. In addition, another DCB specimen was manually opened, and a bridging area of elongated LDPE was observed near the crack tip as illustrated in Figure 31. The complex bi-linear loading curve was likely caused by LDPE yielding/bridging. LDPE near the crack tip was elongated but not broken when the crack was extended. Because LDPE is very plastic, the elongation was retained after specimen closing. During subsequent loading, the bridging area near the crack tip was very loose until the specimen was mostly opened when the bridging area was stretched again. Therefore, the specimen stiffened at the end of the loading cycle. Considering these observations, the initial linear response region was used

to calculate DCB fracture energies with Equations 20 and 21.

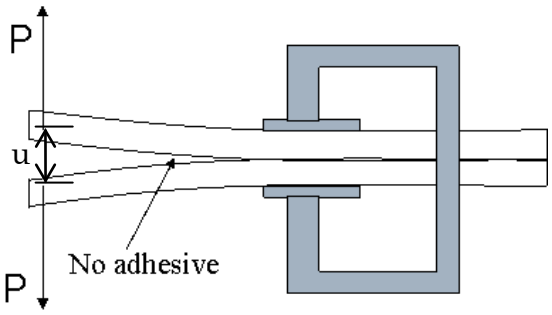

Figure 30. Fractured DCB specimen clamped and loaded

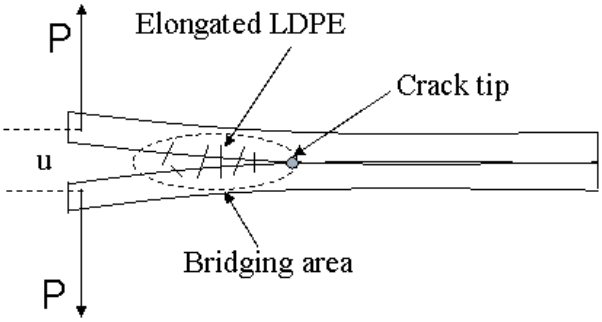

Figure 31. Bridging area of elongated LDPE near the crack tip

4.3.4 Effect of Surface Thermal Deactivation on Fracture Toughness

Figure 32 shows the critical and arrest fracture energies of un-weathered and weathered specimens. Within each sample group, the distribution of fracture energies was tested for normality; the data for NOTR, TM5, TM60W, NOTRW (critical only) and TM5W (critical only) were found to be non-Gaussian. Treatment effects were analyzed both with simple non-paired t-tests (assuming normality) and also with the non-parametric Mann-Whitney test (non-normal). The results were independent of the statistical method and so the following discussion reflects simple t-testing; the criterion for statistical significance was assigned as $\leq p 0.05$. As for un-weathered specimens, the effect of each thermal treatment on fracture

toughness was significant with respect to the next longer treatment time. The fracture energy decreased at TM5 and TM15, and then increased at TM60 near that of NOTR and TM5. As for weathered specimens, NOTRW, TM5W and TM15W didn't exhibit significantly different fracture toughness with an exception that critical fracture energy of TM15W was significantly lower than critical fracture energy of TM5W and NOTRW. The fracture energy of TM60W was significantly higher than other three groups.

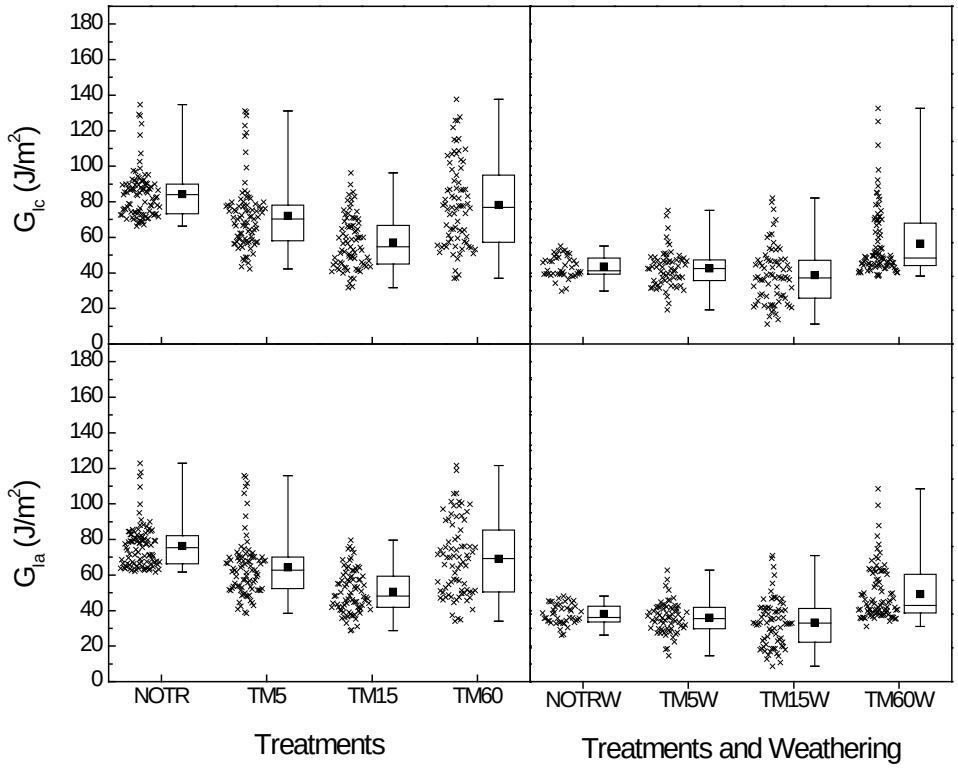

Figure 32. Critical (Top) and arrest (Bottom) fracture energies of un-weathered (Left) and weathered (Right) specimens. Symbols as follows: maximum/minimum (whiskers), 25th and 75th percentile (box), 50th percentile (center line), and the arithmetic mean (black square).

As shown in 4.3.2, the wood surface energy decreased as a function of

thermal treatment. Consequently, wood thermal treatment effectively reduced the surface energy difference between wood and LDPE. With respect to the control specimen toughness, Follrich et al. (2006) observed a steady increase in fracture toughness as the wood thermal treatment time increased. In contrast and in reference to un-weathered specimens, the results found here showed that toughness initially declined and then began trending upward again at the longest thermal treatment times. Follrich et al. (2006) did not investigate the effects of simulated weathering.

As for weathered specimens, for both critical and arrest fracture energy, there was no significant difference among NOTRW, TM5W and TM15W, and TM60W was significantly greater than all these three groups. R represents the percentage of residual fracture energy after weathering. R and its standard deviation, ΔR, are calculated as follows:

$$R = \frac{\mathrm{G_{weathered}}}{\mathrm{G_{control}}}\% \tag{23}$$

$$\Delta R = \mathrm{R}\left(\frac{\Delta \mathrm{G_{control}}}{\mathrm{G_{control}}} + \frac{\Delta \mathrm{G_{weathered}}}{\mathrm{G_{weathered}}}\right) \tag{24}$$

Where $G_{control}, G_{weathered}$ are the average fracture energies of control and weathered specimens; $\Delta G_{control}, \Delta G_{weathered}$ are their standard deviations. As shown in Figure 33, although ΔR increased, R exhibited a clear increasing trend as a function of thermal treatment. Consistent with Follrich et al. (2006), this suggests that the LDPE/wood bond durability is enhanced by wood surface deactivation.

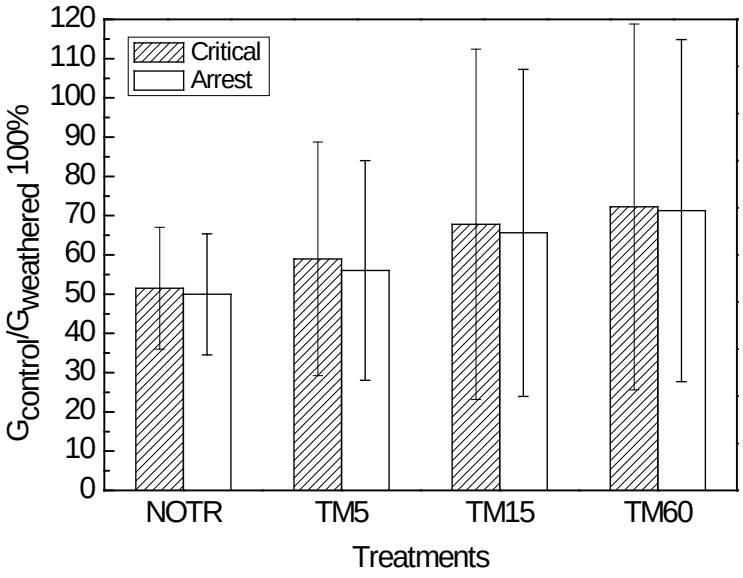

Figure 33. Percentage of fracture energy retained after weathering. Error bars indicate, plus or minus, one standard deviation.

4.4 CONCLUSIONS

As expected, the surface energy of southern yellow pine wood (*Pinus spp*.) was reduced by thermal treatments at 180°C; and the deactivation increased with longer heating times. Regarding un-weathered fracture specimens, lesser degrees of thermal deactivation (lower thermal treatment times) resulted in reduced fracture toughness. However, the longest thermal treatment time (60 min) caused the toughness to increase back to the level of the untreated control specimens. While clearly different from the findings of Follrich et al. (2006), trends for the un-weathered specimens are consistent with improved adhesion at the highest levels of wood deactivation. This is confirmed through the study of weather durability; the greatest weather durability was found for specimens that incurred the highest level of thermal deactivation. Consequently, the

findings in this work support the hypothesis that wood/LDPE adhesion is improved by reducing the surface energy difference between wood and LDPE, and that simple wood thermal treatments should be considered to improve the performance of wood/thermoplastic composite materials.

CHAPTER FIVE: SUMMARY

Mode-I fracture testing was used to test the thermal stability of wood adhesives and the effects of wood deactivation on wood/polyethylene adhesion in the study one and study two. DMA testing was also conduced to investigate the insight of the thermal behavior of wood adhesives in study one. The major finding and conclusions were summarized below:

Study one: Investigating the thermal stability of wood adhesives (PUR and RF) using mode-I fracture testing:

1> The properties of wood (equilibrium moisture content and effective elastic modulus) were reduced after the thermal treatments.

2> PUR is tougher than RF at room temperature. The fracture energy of both adhesives declined after the thermal treatments. Notice that the fracture testing results only reflected the irreversible thermal degradation of the bondline, since the specimens were re-equilibrated after heating.

3> In the DMA testing, the wood grain orientation in the specimen affected the results. "L" specimen result showed that PUR has more thermal softening than RF at 200C^{o}; "R" specimen result showed that RF has more recovery than PUR after cooling.

Study two: The effects of wood deactivation on wood/polyethylene adhesion:

1> The contact angle (water/wood) increased as the heating time increased at 180C^{o}. This also indicated that the wood surface energy decreased as a function of heating time at 180C^{o}.

2> In the fracture testing, the relationship between the loading and the displacement is bilinear which violates the linear fracture mechanics. The bilinear behavior was considered as the effect of bridging area of the elongated polyethylene near the crack tip. The linear region in the initial loading was used to develop the cube root of compliance versus crack length plot.

3> The short time (less than 15 minutes) wood deactivation decreased the fracture energy of wood/polyethylene adhesion, while the long time (60 minutes) wood deactivation increased the fracture energy.

4> The wood deactivation increased the weathering durability in terms of the percentage of toughness remained after the weathering treatment.

REFERENCES

ASTM Standard D2559, 2004, Specification for Adhesives for Structural Laminated Wood Products for Use Under Exterior (Wet Use) Exposure Conditions. ASTM International West Conshohocken, PA, 2004. DOI: 10.1520/D2559-04. www.astm.org.

ASTM Standard D7374, 2008, Standard Practice for Evaluating Elevated Temperature Performance of Adhesives Used in End - Jointed Lumber. ASTM International West Conshohocken, PA, 2008. DOI: 10.1520/D7374-08. www.astm.org.

ASTM Standard D7247, 2007ae1, Standard Test Method for Evaluating the Shear Strength of Adhesive Bonds in Laminated Wood Products at Elevated Temperatures. ASTM International West Conshohocken, PA, 2007. DOI: 10.1520/D7247-07AE01. www.astm.org.

AKYILDIZ, M. H. & ATES, S. 2008. Effect of Heat Treatment on Equilibrium Moisture Content (EMC) of Some Wood Species in Turkey. *Research Journal of Agriculture and Biological Sciences,* 4**,** 660-665.

BARNES, D. 2000. An Integrated Model of the Effect of Processing Parameters on the Strength Properties of Oriented Strand Wood Products. *Forest Products Journal,* 50**,** 33-42.

BARNES, D. 2001. A Model of the Effect of Strand Length and Strand Thickness on the Strength Properties of Oriented Wood Composites. *Forest Products Journal,* 51**,** 36-46.

BLACKMAN, B., DEAR, J. P., KINLOCH, A. J. & OSIYEMI, S. 1991. The Calculation of Adhesive Fracture Energies from Double-Cantilever Beam Test Specimens. *Journal of Materials Science Letters,* 10**,** 253-256.

CHRISTIANSEN, A. W. 1990. How Overdrying Wood Reduces Its Bonding to Phenol-Formaldehyde Adhesives - a Critical-Review of the Literature .1. Physical Responses. *Wood and Fiber Science,* 22**,** 441-459.

CHRISTIANSEN, A. W. 1991. How Overdrying Wood Reduces Its Bonding to Phenol-Formaldehyde Adhesives - a Critical-Review of the Literature .2. Chemical-Reactions. *Wood and Fiber Science,* 23**,** 69-84.

CONRAD, M. P. C., SMITH, G. D. & FERNLUND, G. 2004. Fracture of Wood Composites and Wood-adhesive Joints: A Comparative Review. *Wood and Fiber Science,* 36**,** 26-39.

DEL MENEZZI, C. H. S., DE SOUZA, R. Q., THOMPSON, R. M., TEIXEIRA, D. E., OKINO, E. Y. A. & DA COSTA, A. F. 2008. Properties after Weathering and Decay Resistance of a Thermally Modified Wood Structural Board. *International Biodeterioration & Biodegradation,* 62**,** 448-454.

DEL MENZZI, C. H. S. & TOMASELLI, I. 2005. Contact Chermal Post-treatment of Oriented Strandboard to Improve Dimensional Stability: Apreliminary Study. *Holz Roh-Werkst*,64, 212-217

DOWLING, N.E. 2007. MECHANICAL BEHAVIOR OF MATERIALS,. Prentic Hall, Third Edition.

EBEWELE, R., RIVER, B. & KOUTSKY, J. 1979. Tapered Double Cantilever Beam Fracture Tests of Phenolic-Wood Adhesive Joints .1. Development of Specimen Geometry - Effects of Bondline Thickness, Wood Anisotropy and Cure Time on Fracture Energy. *Wood and Fiber,* 11**,** 197-213.

EBEWELE, R. O., RIVER, B. H. & KOUTSKY, J. A. 1980. Tapered Double Cantilever Beam Fracture Tests of Phenolic-Wood Adhesive Joints .2. Effects of Surface-Roughness, the Nature of Surface-Roughness, and Surface Aging on Joint Fracture Energy. *Wood and Fiber,* 12**,** 40-65.

EBEWELE, R. O., RIVER, B. H. & KOUTSKY, J. A. 1982. Relationship between Phenolic Adhesive Chemistry, Cure and Joint Performance .1. Effects of Base Resin Constitution and Hardener on Fracture Energy and Thermal Effects during Cure. *Journal of Adhesion,* 14**,** 189-217.

EBEWELE, R. O., RIVER, B. H. & KOUTSKY, J. A. 1986a. Relationship between Phenolic Adhesive Chemistry and Adhesive Joint Performance - Effect of Filler Type on Fraction Energy. *Journal of Applied Polymer Science,* 31**,** 2275-2302.

EBEWELE, R. O., RIVER, B. H. & KOUTSKY, J. A. 1986b. Wood Processing Variables and Adhesive Joint Performance. *Journal of Applied Polymer Science,* 32**,** 2979-2988.

FOLLRICH, J., MULLER, U. & GINDL, W. 2006. Effects of Thermal Modification on the Adhesion Between Spruce Wood (Picea abies Karst.) and a Thermoplastic Polymer. *Holz Als Roh-Und Werkstoff,* 64**,** 373-376.

GAGLIANO, J. M. & FRAZIER, C. E. 2001. Improvements in the Fracture Cleavage Testing of Adhesively-bonded Wood. *Wood and Fiber Science,* 33**,** 377-385.

GERHARDS, C. C. 1979. Effect of High-Temperature Drying on Tensile-Strength of Douglas-Fir 2 by 4s. *Forest Products Journal,* 29**,** 39-46.

GERHARDS, C. C. 1983. Effect of High-Temperature Drying on Bending Strength of Yellow-Poplar 2-by-4s. *Forest Products Journal,* 33**,** 61-67.

GUNNELLS, D. W., GARDNER, D. J. & WOLCOTT, M. P. 1994. Temperature-Dependence of Wood Surface-Energy. *Wood and Fiber Science,* 26**,** 447-455.

HAKKOU, M., PETRISSANS, M., ZOULALIAN, A. & GERARDIN, P. 2005. Investigation of Wood Wettability Changes During Heat Treatment on the Basis of Chemical Analysis. *Polymer Degradation and Stability,* 89**,** 1-5.

KOCH, P. 1971. Process for Straightening and Drying Pine 2 by 4s in 24 Hours. *Forest Products Journal,* 21**,** 17-24.

KOCH, P. 1976. Strength of Southern Pine Lumber Dried at High Temperature. In: Proceedings, Research conference on high-temperature drying effects on mechanical properties of softwood lumber; 1976 February 25-26; Madison, WI: U.S. Department of Agriculture, Forest Service, Forest Products Laboratory: P. 38-49

LADELL, J. L. 1956. High Temperature Drying of Yellow Birch. *Forest Products Journal,* 6**,** 470-475.

LAI, Y. H. & DILLARD, D. A. 1997. Using the Fracture Efficiency to Compare Adhesion Tests. *International Journal of Solids and Structures,* 34**,** 509-525.

LEVAN, S. L. & WINANDY, J. E. 1990. Effects of Fire Retardant Treatments on Wood Strength - a Review. *Wood and Fiber Science,* 22**,** 113-131.

LIM, W. W., HATANO, Y. & MIZUMACHI, H. 1994. Fracture-Toughness of Adhesive Joints .1. Relationship between Strain-Energy Release Rates in 3 Different Fracture Modes and Adhesive Strengths. *Journal of Applied Polymer Science,* 52**,** 967-973.

LIM, W. W. & MIZUMACHI, H. 1995. Fracture-Toughness of Adhesive Joints .2. Temperature and Rate Dependencies of Mode-I Fracture-Toughness and Adhesive Tensile-Strength. *Journal of Applied Polymer Science,* 57**,** 55-61.

LOPEZ-SUEVOS, F. & FRAZIER, C. E. 2006. Fracture Cleavage Analysis of PVAc Latex Adhesives: Influence of Phenolic Additives. *Holzforschung,* 60**,** 313-317.

MACKAY, J.G.G. 1976. Effect of High Temperature Kiln-drying on Lumber Properties. In: Proceedings, Research conference on high temperature drying effects on mechanical properties of softwood lumber. Madison, WI: U.S. Department of Agriculture, Forest Service, Forest Products Laboratory: 73-78.

MIJOVIC, J. S. & KOUTSKY, J. A. 1979. Effect of Wood Grain Angle on Fracture Properties and Fracture Morphology of Wood-Epoxy Joints. *Wood Science,* 11**,** 164-168.

MURPHY, J. F. 1986. Strength and Stiffness Reduction of Large Notched Beams. *Journal of Structural Engineering-Asce,* 112**,** 1989-2000.

NUSSBAUM, R. M. & STERLEY, M. 2002. The Effect of Wood Extractive Content on Glue Adhesion and Surface Wettability of Wood. *Wood and Fiber Science,* 34**,** 57-71.

PODGORSKI, L., CHEVET, B., ONIC, L. & MERLIN, A. 2000. Modification of Wood Wettability by Plasma and Corona Treatments. *International Journal of Adhesion and Adhesives,* 20**,** 103-111.

RAKESTRAW, M. D., TAYLOR, M. W., DILLARD, D. A. & CHANG, T. 1995. Time Dependent Crack Growth and Loading Rate Effects on Interfacial and Cohesive Fracture of Adhesive Joints. *Journal of Adhesion,* 55**,** 123-149.

REITERER, A., 2001. The Influence of Temperature on The Mode I Fracture Behavior of Wood. *Journal of Materials Science Letters*, 20, 1905-1907

RIVER, B. H. & OKKONEN, E. A. 1993. Contoured Wood Double Cantilever Beam Specimen for Adhesive Joint Fracture Tests. *Journal of Testing and Evaluation,* 21**,** 21-28.

RIVER, B. H., SCOTT, C. T. & KOUTSKY, J. A. 1989. Adhesive Joint Fracture-Behavior during Setting and Aging. *Forest Products Journal,* 39**,** 23-28.

SALAMON, M. 1969. High Temperature Drying and its Effect on Wood Properties. *forest Products Journal,* 19**,** 27-34.

SASAKI, H., MCARTHUR, E. & GOTTSTEIN, J. W. 1973. Maximum Strength of End-grain to End-grain Butt Joints. *Forest Products Journal,* 23**,** 48-54.

SERNEK, M., KAMKE, F. A. & GLASSER, W. G. 2004. Comparative Analysis of

Inactivated Wood Surfaces. *Holzforschung,* 58**,** 22-31.

SHI, S. Q. & GARDNER, D. J. 2001. Dynamic Adhesive Wettability of Wood. *Wood and Fiber Science,* 33**,** 58-68.

TJEERDSMA, B. F., BOONSTRA, M., PIZZI, A., TEKELY, P. & MILITZ, H. 1998. Characterisation of Thermally Modified Wood: Molecular Reasons for Wood Performance Improvement. *Holz Als Roh-Und Werkstoff,* 56**,** 149-153.

WHITE, M. S. 1977. Influence of Resin Penetration on Fracture Toughness of Wood Adhesive Bonds. *Wood Science,* 10**,** 6-14.

WHITE, M. S. & GREEN, D. W. 1980. Effect of Substrate on the Fracture-Toughness of Wood-Adhesive Bonds. *Wood Science,* 12**,** 149-153.

WHITE, R. H. & DIETENBERGER, M. A. 2001. Wood Products: Thermal Degradation and Fire. *Encyclopedia of Materials: Science and Technology,* 9712-9716

WINANDY, J. E. & KRZYSIK, A. M. 2007. Thermal Degradation of Wood Fibers During Hot-pressing of MDF Composites: Part I. Relative Effects and Benefits of Thermal Exposure. *Wood and Fiber Science,* 39**,** 450-461.

WINANDY, J. E. & LEBOW, P. K. 2001. Modeling Strength Loss in Wood by Chemical Composition. Part I. An Individual Component Model for Southern Pine. *Wood and Fiber Science,* 33**,** 239-254.

WINANDY, J. E. 1994. Effects of Treatment, Incising, and Drying on Mechanical Properties of Timber. U.S. Department of Agriculture, Forest Service, Forest Products Laboratory. USDA Forest Serv. Gen. Tech. Rep. FPL-GTR 94: 371-378

YAO, J. & TAYLOR, F. 1979. Effect of High-Temperature Drying on the Strength of Southern Pine Dimension Lumber. *Forest Products Journal,* 29**,** 49-51.

YOUNGQUIST, J. A., MYERS, G. C. & MURMANIS, L. L. 1987. Resin Distribution in Hardboard - Evaluated by Internal Bond Strength and Fluorescence Microscopy. *Wood and Fiber Science,* 19**,** 215-224.

APPENDIX A: TRANSVERSE SHEAR STRESS AT ADHESIVE LAYERS IN THE DMA SPECIMENS

The single cantilever testing of bonded specimens is like as shown in figure A1 (a). If the three laminae are not bonded with adhesives, under the vertical shear stress, there would be slippages between layers as shown in figure A1 (b). With bonding two layers together, the slippages are avoided by the horizontal shear stress provided by the adhesives as shown in figure A1 (c). In other words, in the single cantilever testing, the adhesive layers are horizontally sheared by the stress τ developed from the vertical shear stress V.

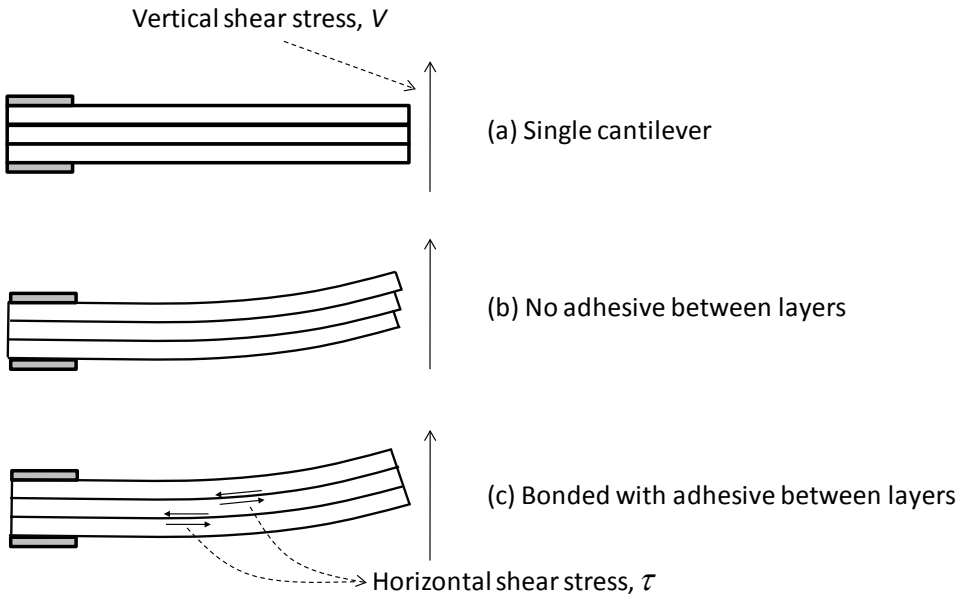

Figure A1: Horizontal shear stress in adhesive layer

In the testing, the vertical shear force caused a non-constant moment distribution as shown in figure A2 (a), and the horizontal shear stress is developed by the difference of the moment as shown in figure A2 (b). At any

layer *ab*, the total force to right, f1, is greater than the total force to left, f2, because M1 is greater than M2. Thus, the shear force applied to the layer *ab* equals to the difference of f1 and f2.

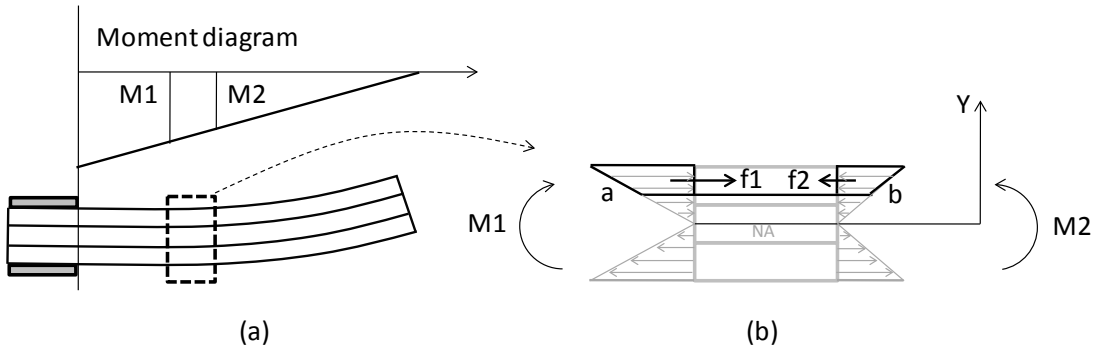

Figure A2: Horizontal shear stress developed from vertical shear stress

The horizontal shear stress is calculated as below:

$$\tau = \frac{\mathrm{VQ}}{I\mathrm{t}} \tag{A1}$$

where V is the vertical shear stress; I is the moment of inertia; t is the width of the beam; Q is the first moment of the area varies with the distance (y) from the neutral axis as shown in figure A3.

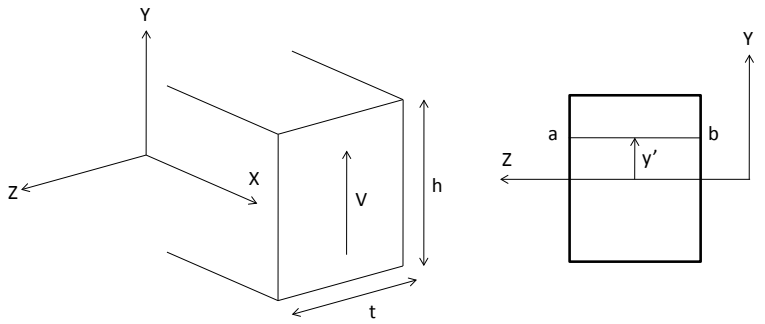

Figure A3: Calculation of the first moment of the area

The Q is calculated as below:

$$Q = \frac{\mathrm{t}}{2}\left(\frac{\mathrm{h}^2}{2} - \mathrm{y}'^2\right) \tag{A2}$$

Combine equation A1 and A2, equation A1 reduces to below:

$$\tau = \frac{\mathrm{V}}{2I}\left(\frac{\mathrm{h}^2}{4} - \mathrm{y}'^2\right) \tag{A3}$$

From equation A3 the τ distribution is plotted in figure A4.

Figure A4: Transverse shear stress distribution